NASA Contractor Report 177552

The Aerodynamic Design of the Oblique Flying Wing Supersonic Transport

Alexander J. M. Van Der Velden and Ilan Kroo
Stanford University, Palo Alto, California

Prepared for
Ames Research Center
Cooperative Agreement NCA2-343
June 1990

National Aeronautics and
Space Administration

Ames Research Center
Moffett Field, California 94035-1000

TABLE OF CONTENTS

Page

1.

1.1 Introduction 1

1.2 Summary 3

2. CONCEPTUAL AERODYNAMIC DESIGN 5

2.1 Objectives 5

2.2 A Semi-empirical Model for Conceptual Design 6

2.3 Payload Size Affecting Wing Geometry 9

2.4 The Impact of Technology on Economy 11

2.5 Factors Determining Wing Size 12

2.6 Effect of Cruise Mach number, Sweep and Altitude 16

3. DEVELOPMENT OF THE AIRFOIL 19

3.1 Objectives and Requirements 19

3.2 Baseline Airfoil Design 19

3.3 Thickness Trade-off 28

4. THREE DIMENSIONAL WING DESIGN 31

4.1 General considerations 31

4.2 Wing Planform and Basic Thickness Distribution 31

4.3 From a Two-Dimensional Pressure Distribution to a Three-Dimensional Wing 34

4.4 The Calculation of Drag with Coarse Paneling 42

4.5 Evaluation of the Forces and Moments 49

4.6 Control Authority 55

5. CONCLUSIONS 56

REFERENCES 59

SOFTWARE REFERENCES 62

ACKNOWLEDGEMENTS 62

Nomenclature

a	local velocity of sound normalized with respect to the freestream velocity
a ,b	semi-minor, and semi-major axis of elliptic wing
AR	aspect ratio
(dt/dx)/2	half thickness distribution slope of a panel
dz/dx	mean line slope of a panel
h	altitude
K	lift-dependent drag factor
KO	Sears Haack factor
M	freestream Mach number
OFW	Oblique Flying Wing
R	range
Re	Reynolds number
S	Wing area
t/c	thickness-to-chord ratio
u,v,w	perturbation velocity in x,y,z-direction normalized with respect to the freestream velocity
W	weight
U	total velocity normalized with respect to the freestream velocity

Greek symbols

β	Prandtl's compressiblity coefficient: $\sqrt{1-M^2}$
Λ	panel $1/4c$ sweep angle
$1/4\ c$	quarter chord line of the panel
Θ	dihedral, positive with increasing z and y
η	total propulsive efficiency as used in the Brequet relation
ψ	slew angle (90^o-Λ)

indices:

dd	drag divergence
EAS	equivalent air speed
f	fuel
l	local
n	number of passengers
p	payload, pressure
pp	powerplant

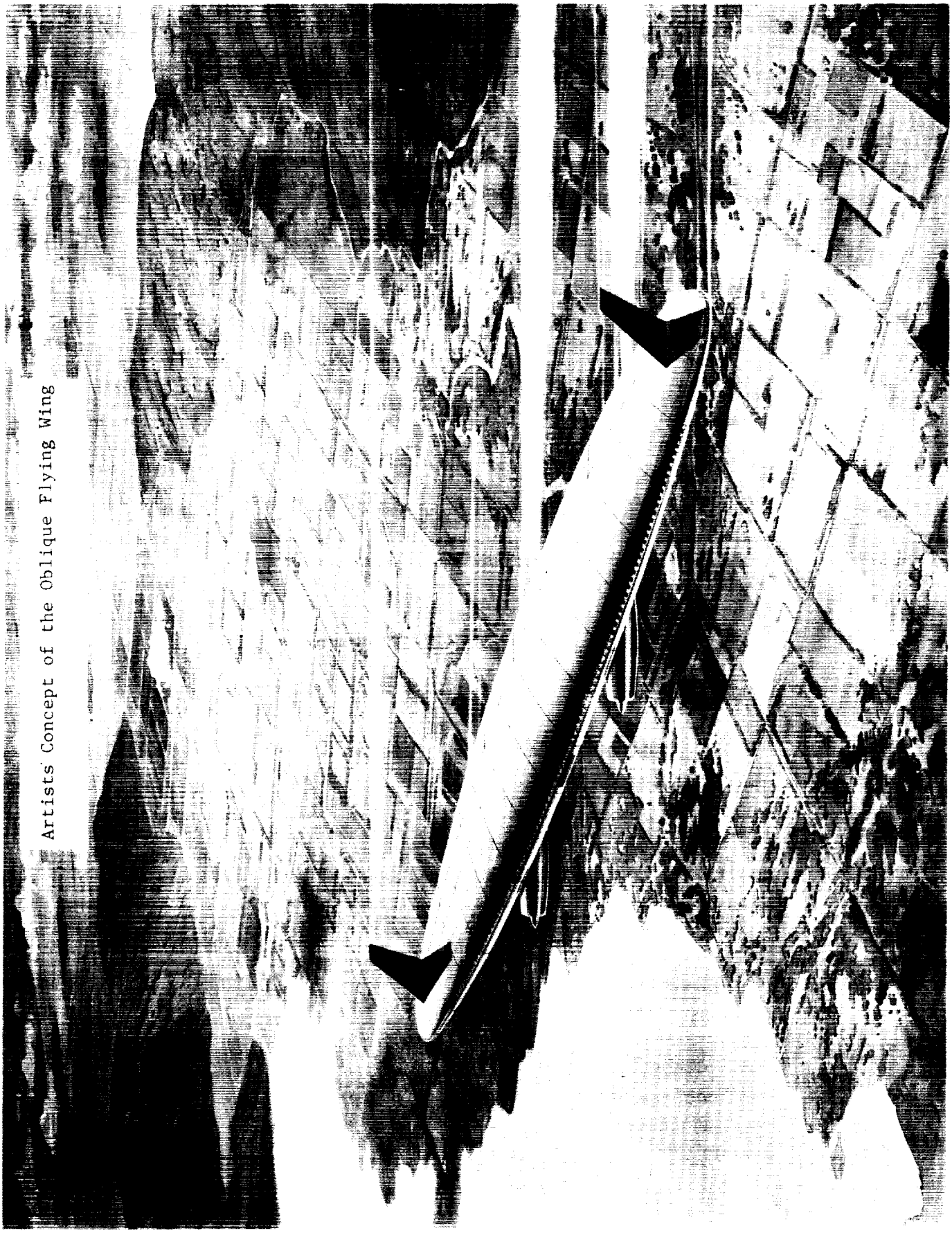

Artists' Concept of the Oblique Flying Wing

Fig. 1

1.1 Introduction

Background and Present Work

In the late fifties R.T. Jones [25, 1, 13] suggested that aircraft with asymmetrically swept wings (or oblique wings) would offer many advantages over aircraft with conventional wing design at high transonic and low supersonic speeds. The primary advantages of the oblique wing arise from its improved structural arrangement and its reduced subsonic and transonic drag. Recent work by Rockwell and NASA engineers [26, 29, 20] has provided the tools needed for studying the oblique wing for transonic and low-supersonic speeds in greater detail.

In this work we extend these analytic capabilities and apply them to the aerodynamic design of oblique flying wings. Figure 1. shows an artist's impression of the oblique flying wing and Fig. 2 shows a three-view of the baseline Oblique Flying Wing. The baseline wing has a near elliptic planform, which can be swept from 35^o at takeoff to 70^o in cruise. The passengers are located at the center of the planform inside the wing structure. Work done by Van der Velden on NASA grant NAG-2-471 [41] indicated that this configuration could provide economical supersonic transportation if the theoretical minimum drag based on potential flow can be obtained.

Prediction Methods

Up to now, numerical calculations and windtunnel tests up to Mach 1.4 have been published. Beyond Mach 1.4 only the theoretical minimum potential drag for this configuration is known. At a higher Mach number, the occurrence of shocks and flow separation may limit the applicability of potential flow methods, and we therefore require analysis tools which include these effects. Though the Navier-Stokes equations could be used to analyze the configuration, it is not yet possible to solve for the geometry on the basis of a pressure distribution with this method. Apart from this limitation, these solutions are very time consuming for 3D flow. For 2D flow, fairly rapid solvers exist and they can be used to analyze and design sections. The 3D wing can be analyzed with the Prandtl-Glauert equation for supersonic Mach numbers from 1.5 to 3.0 if the shear-layer is thin and the shocks are weak. The high Reynolds numbers assure that the shear layer is thin for the attached flow, while the section data is used to identify the local normal Mach number and recovery distributions that are separation and shock-free.

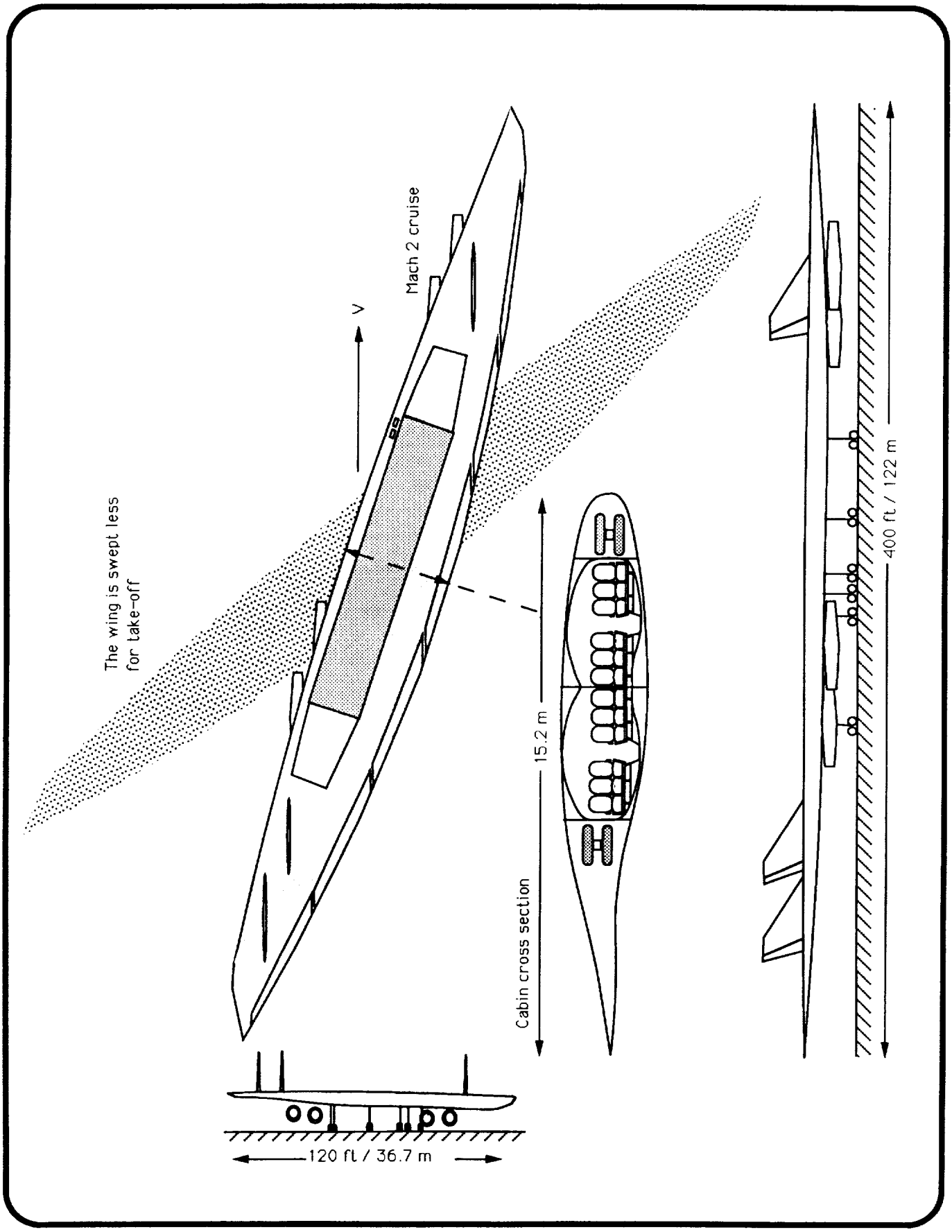

Fig. 2: Oblique Flying Wing by Alex van der Velden

1.2 Summary

This study describes the aerodynamic design of a thick Mach 2 Oblique Flying Wing (OFW). A preliminary design analysis indicates that the best payload fractions are obtained for a takeoff wing loading of 2 kN/m^2 at an altitude of 16 km and an unswept aspect ratio of 10.

An optimization study projects that the highest payload fraction is achieved for a 16% thick root airfoil. This airfoil, and the airfoil family derived from it, are designed with ARC2D, a Navier-Stokes code. The OFW airfoil family allows a good utilization of the passenger cabin and it achieves the required trimmed lift at the 0.32 chord location. This is the rearmost location at which artificial stability and control by a narrow trailing edge flap can be achieved.

Each member of the airfoil family has a different thickness and trimmed drag divergence lift. By selecting the right airfoil at each station along the span it is possible to achieve a Sears-Haack area distribution and an elliptic lift distribution. Such distributions minimize the potential flow drag.

We present a new method for determining a wing's design pressure distribution based on airfoil data. The pressure distribution is calculated from the potential flow velocity perturbations for a given thickness distribution and the prescribed vorticity. The vorticity in *supercritical* wing regions is based on airfoil transonic normal Mach numbers and includes the influence of local sweep, taper and three-dimensional induced velocities, so that the appearance and the strength of the shock waves can be expected to resemble those of the airfoil. The vorticity in *subcritical* wing regions is scaled first with simple sweep theory, and then to achieve the desired load distribution. The vorticity distribution is then used to solve for the wing's camber with an inverse panel code. The induced velocity perturbations of this cambered wing are used in the next iteration.

The potential drag of the wing designed in this fashion with a panel code was very close to the ones given by R.T. Jones [2] and J.H.B. Smith [3] for a minimum drag oblique wing. The method was also successful in constraining the local normal Mach numbers to the values that would produce only weak shocks. The moment and force characteristics of the wing at the design condition indicate that the wing could be trimmed and controlled without high drag penalties.

2 CONCEPTUAL AERODYNAMIC DESIGN

2.1 Objectives

Though there is no one set of missions that can be specified for a new aircraft, it is possible to indicate which range of missions is most likely to result in an economically competitive aircraft. The following section describes the rationale for the selection of mission parameters in this work.

Cruise Mach number

We investigated designs optimized for cruise speed between Mach 1.2 and 3.0. The most attention was paid to the Mach 2 cruise speed. At this Mach number the technology risk is moderate and the cost of development can be acceptable. At Mach 3 the aircraft would be twice as expensive [12].

Payload

Today a proven market exists for long range transports with up to 550 passengers or 100,000 kg payload. Within the geometric constraints posed by the accommodation of passengers there is almost no difference in size between a 1-, and a 100-passenger flying wing, and therefore only aircraft with a high payload will be considered.

Existing payloads are:

- 118 pax (Concorde): Too small to be a successful flying wing, but would require the least initial investment.
- 247 pax (SST): The target American payload for a supersonic transport. However, in view of the growth of the market such a transport may still be too small when it enters the market in 20 years.
- 452 pax (B747): Probably the best payload for a flying wing, but would require the highest initial investment.

Range

In this study a design range of 5000 nautical miles or 9000 km was used, the current range of a B747 with maximum payload. Because all proposed Oblique Flying Wings have a similar level of technology, a good optimization criterion is the payload to takeoff weight

ratio for a given mission [15]. On closer inspection this criterion encompasses both fuel efficiency and depreciation of the airframe. This economic criterion was used to establish at an early phase which configurations should be developed further, without the need of dubious cost-analyses.

2.2 A Semi-empirical Model for the Conceptual Design

The semi-empirical methods developed in by A. Van der Velden in References 4 and 41 assume 1970s technology for all aircraft components. In this way, an unbiased comparison with existing aircraft was possible. A short list of the basic assumptions and methodologies is given below:

Geometry

To accommodate passengers comfortably, certain minimum geometric requirements have to be satisfied. We selected a minimum passenger cabin aisle height of 75"=191 cm, and a sitting height of 56"=142 cm. We also required that the cargo holds have an internal height of at least 45" with a 6" clearance in order to allow the aircraft to carry the belly containers of today's domestic subsonic transports as well as a range of IATA containers.

The required floor area per passenger is about 0.6 m^2 for an economy layout, and 0.7m^2 for a normal layout according to empirical data from Ref. 5. The cargo floor to passenger floor ratio is approximately 1 to 4 for the configuration presented in Fig.1 .

Aerodynamics

The friction drag was calculated for each component based on the Prandtl Schlichting equation. This equation assumes a fully turbulent boundary layer as a function of Mach number and Reynolds number for a Prandtl number of 0.9:

$$Cf_{component}=\frac{0.455}{1+0.18M^2}\left(Log_{10}\left[\frac{Re_{component}}{(1+0.18M^2)^{2.8}}\right]\right)^{-2.58}$$

We added a form drag according to Ref. 5 pp. 499-501, assuming transition at 5% from the leading edge.

The linear, supersonic, volume-dependent wave drag was based on J.H.B Smith's method

given in Ref. 3. The lift-dependent drag was taken to be equal to the minimum lift-dependent drag of an elliptic oblique wing with full leading edge suction, according to R.T. Jones [2]. CD_{wave} is the volume dependent wave drag and CD_{lift} is the lift-dependent drag as a function of Mach number,slew angle ψ and root chord thickness t from the expressions developed in Refs. 2 and 3:

$$CD_{wave}=\frac{t^2}{A^2}Re\left\{\frac{\beta-\left(M+i\frac{A}{B}\right)\left(M+2i\frac{A}{B}\right)}{\left[\beta^2-\left(M+i\frac{A}{B}\right)^2\right]^{3/2}}\right\} \qquad CD_{lift}=\frac{CL^2}{4}Re\sqrt{\left[\beta^2-\left(M+i\frac{A}{B}\right)^2\right]}$$

$$A=\frac{ab}{B} \qquad B=\sqrt{a^2\cos^2\psi+b^2\sin^2\psi} \qquad M=\frac{\left[b^2-a^2\right]\sin\psi\cos\psi}{B^2}$$

The wave drag of the other components was calculated from Wards' [28] transfer rule. In particular, we approximated the drag of the nacelles in the presence of the wing by using Swan's [42] estimate. The spillage drag coefficient was based on the engine mass flow ratio, as suggested by Ref. 7. The skin roughness drag was based on a material grain size of 17μm, turbulent flow and the method of Ref. 43. We estimated the drag from fabrication type roughness from Ref. 46. Finally, the flap and systems drag were calculated with the method of Refs 44 and 45.

Weight

As a guideline throughout the weight calculations Torenbeek's [5] itemized weight penalty method was used. In Ref. 41 this method was adapted for the OFW. The pressure differential gave the critical load for the passenger cabin, and the bending moment gave the critical load for the outer wing panels. To convert these loads into structural weight, only aluminum alloys or materials with the same maximum stress to weight ratio as aluminum alloys were considered.

The fuel weight was calculated from the Breguet equation. We added to the cruise fuel weight a range increment of 1200 km for diversions and a 7% allowance for climb:

$$w_f=1.07\left[1-\exp\left(\frac{-0.23(R+1.2)}{(\eta L/D)}\right)\right]w_{to} \qquad \text{with R in Mm}$$

Instead of using the usual Class II itemized weight penalty method and iterating to obtain the correct weight, we can model the takeoff weight more conveniently by expressing the takeoff weight by using a Class I method:

$$w_{to} = w_{fixed} + \frac{\partial wpp}{\partial(\frac{wto}{L/D})} \frac{w_{to}}{L/D} + \frac{\partial woe}{\partial wto} w_{to} + \frac{\partial woe}{\partial S} S + \frac{\partial woe}{\partial n} n + w_p + w_f$$

The variables and their values are given below:

w_{fixed}	fixed weight items	500 kg
$\frac{\partial woe}{\partial S}$	variation of empty weight with wing area. This includes midsection, outboard panels, flaps and vertical tails.	35.2 kg/m^2
$\frac{\partial wpp}{\partial(\frac{wto}{L/D})}$	variation of nacelle and engine weight with lift-to-drag and takeoff weight at h=16500m cruise. This includes nacelles, pivots and engines: An expression for the power plant weight fraction with constant total weight and variable altitude is given in section 3.3.	1.02
$\frac{\partial woe}{\partial wto}$	variation of the empty weight with takeoff weight. This includes the gear, apu, instruments, and hydraulic, pneumatic, electrical and anti-icing systems.	0.071
$\frac{\partial woe}{\partial n}$	variation of the empty weight with number of passengers. This includes the operational items, furnishings and equipment, and airconditioning.	60

Propulsion

We assumed a conventional turbofan layout with 3D inlet and variable geometry exhaust. Engine performance was estimated from isentropic work relations which were corrected with realistic efficiency factors. FAR 36 stage 3 Noise requirements determined the bypass ratio of the engines. The noise levels were determined by.an empirical relation from Ref. 4. between jet exhaust velocity and velocity profile.

Stability and Control

Ref. 41 indicated that sufficient control authority over an unswept OFW existed at a center of gravity location of 32% mac with a 10% simple slotted trailing edge flap actuated by a stability augmentation system at V_{EASmin}=130 m/s during climb. Vertical tailplanes with a

planform area of 5% of the wing planform area located near the wing tips provide adequate control authority in case of engine failure.

2.3 Payload Size Affecting Wing Geometry

The wing can be tailored in such a way that we obtain a Sears-Haack area distribution, elliptic lift and maximum utilization of the volume for payload and fuel. This was accomplished with the following approach:

The total empty weight of the OFW for a given payload relates directly to the wing planform area. So the maximum payload fraction is obtained at the maximum payload floor fraction Sp/S. For a given payload the required wing size can be determined by the assumption of the Sears Haack Area distribution and given minimum internal dimensions to accommodate the payload.

Fig. 2.1 shows the available fraction of the planform area used by passengers and cargo plotted against the maximum root section thickness and the root taper ratio of 0.7 for an assumed NACA airfoil. The taper ratio of 0.7 was selected because it gave the least variation in thickness-to-chord ratio over the span of the passenger cabin. Section 2.5 will show that the design is constrained by the maximum local thickness-to-chord ratio. It is therefore advantageous to use this maximum over as large an inboard span as possible to maximize the available payload area and volume. Starting with a root chord of given thickness, the wing is tapered up to the point where the internal height is less than that required to store cargo, from this point on, the wing is tapered so it joins with the tip geometry. The tip geometry is similar to that of the NASA oblique wing demonstrator [20].

To provide some idea of the aisle layout, a 15.2 m root chord wa introduced. This value was used for the baseline aircraft of Fig. 1. Fig 2.1 shows that, for a given payload, the required area of the flying wing increases significantly below a root thickness of 2.2 m, but it does not decrease significantly beyond a root thickness of 2.4 m. If we consider the necessity of an additional aisle, then a thickness of 2.3 m becomes even more appealing. It is also clear that the volume, and hence the wave drag, does increase quickly for a vehicle that becomes smaller but increases in volume. This would be the case if we where to use a higher thickness.

The preceding data is not adequate to allow us to decide on a final geometry for the aircraft. However, it has been shown that for an initial taper around 0.7 and a maximum thickness around 2.3 m a good utilization of the available volume and area is achieved. In Section 3.3 we will present further proof of the validity of this choice.

Fig. 2.1: OFW planform utilization

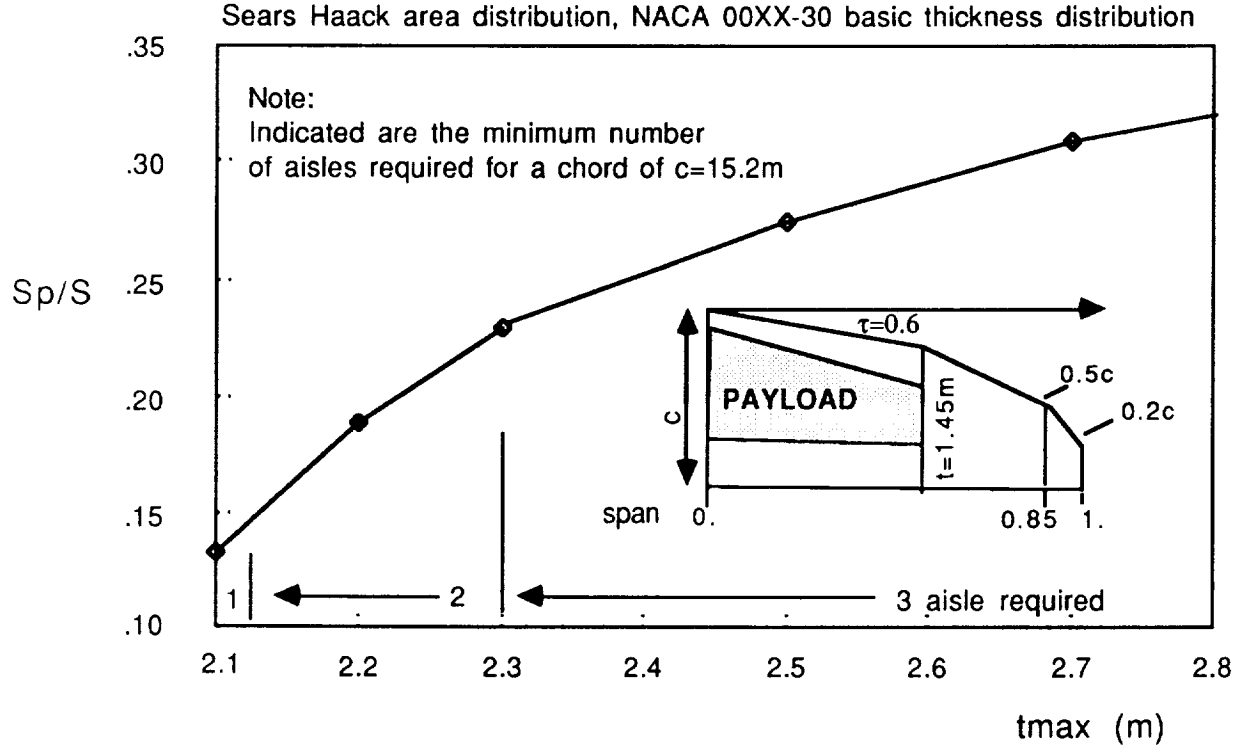

Fig 2.2: Effect of technology on payload fraction

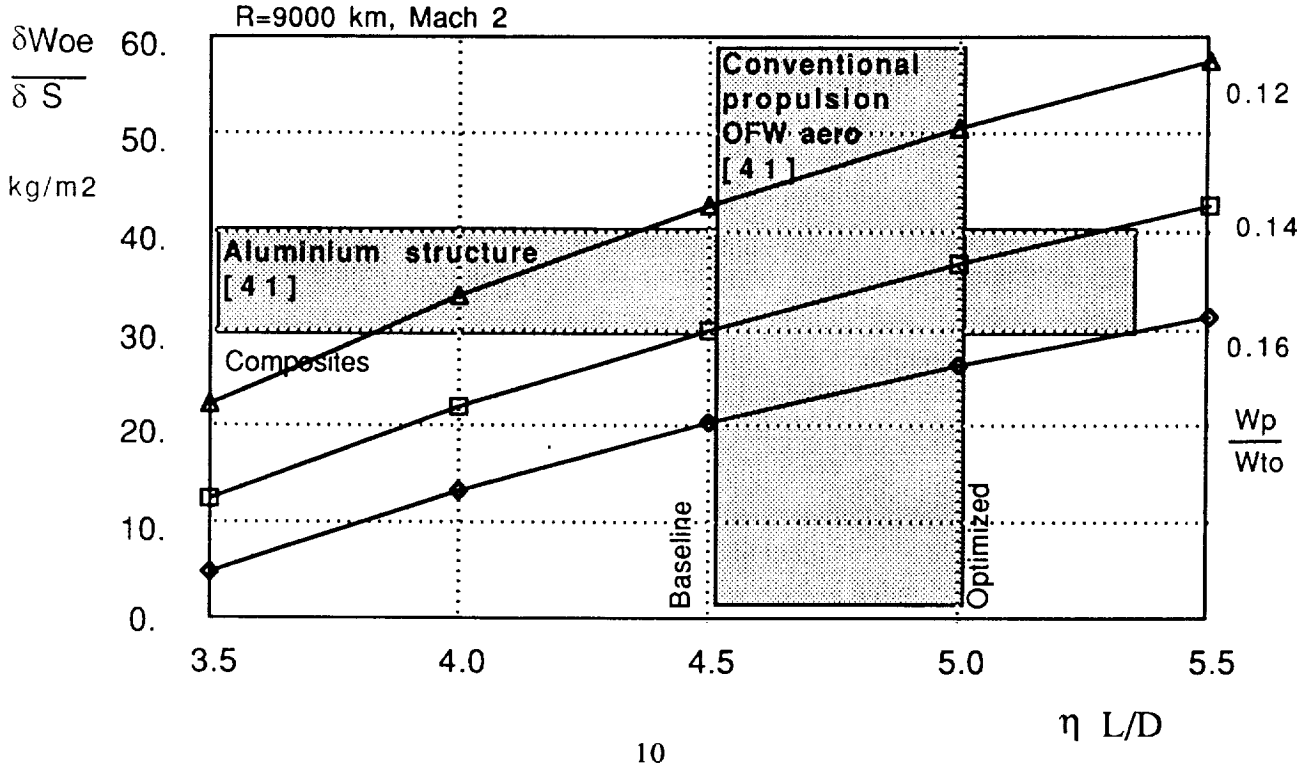

2.4 The Impact of Technology on Economy

For conventional aircraft, wing loading is a powerful means to change the aircraft's performance. For an oblique flying wing designed to accommodate passengers, this is not the case, and the range of available wing loadings will be primarily a function of desired operating costs.

One way of looking at the economy of a configuration is through parameters such as payload fraction, fuel used per passenger and structural weight per passenger. As discussed by Torenbeek [15] and Van der Velden [12] the payload fraction has the most influence on the aircraft's economic performance since it contains terms expressing the fuel and depreciation cost in about the right ratio. For a supersonic aircraft with a range of 9000 km a payload fraction of at least 12% should be achieved if the aircraft is going to be economically competitive. A payload fraction of 16% represents a fraction not yet obtained by subsonic technology.

In section 2.3 a maximum thickness of 2.3 m was selected and this corresponds to a payload floor fraction of about 0.235. In section 2.2 the area required for one passenger and cargo was found to be 0.8 m^2 for a half normal, half economy layout. The total weight of a passenger and cargo is about 97 kg, which results in a payload loading (pl) of 119.38 kg/m^2.

The required wing area can now be expressed as: $S = {}^{w_p}/_{(pl\ Sp/S)}$

Inverting and dividing by the takeoff weight gives: ${}^{w_{to}}/_{S} = 28.0\ [{}^{m_{to}}/_{m_p}]$

The expression found for the wing loading results in values of the wing loading between 233 and 175 kg/m^2 for target payload fractions between 12% and 16% respectively. To investigate whether such wingloadings can actually be achieved from a technological perspective, we simplified the class I weight model further by expressing the first three terms as a fraction of maximum takeoff weight:

$$w_{to} = 0.179\ w_{to} + \frac{\partial w_{oe}}{\partial S} S + 1.69\ w_p + w_f$$

Fig. 2.2 shows that for a target payload fraction of between 12% and 16% and its appropriate wing loading, only current technology is required. The variation of operating empty weight with wing area can also be interpreted as an average structural weight per unit

area multiplied by the ratio of total wetted area to the reference area. Since spanloading wings do not exhibit a relative increase in structural weight with an increase in size, this number represents a level of structural technology independent of size. The structural weight per unit area varies from component to component, but for the OFW described in Ref. 41 an average value of 35 kg/m2 was found. An earlier parametric study of 7 supersonic designs [18] found that their average structural specific wing weight was 38 kg/m^2 within a 10% range.

This means that the OFWs of interest will have maximum wing loadings of around 200 kg/m2 for a range of 9000 km and a payload fraction of 14% using only conventional technology. This is the same payload fraction that the B747 achieves and more than 50% higher than is projected by the current HSCT [16] studies. It is also interesting to note that this number is not very sensitive to expected changes in technology level.

2.5 Factors Determining Wing Size

The range of possible wing sizes for a given payload is limited by a number of constraints:

Passenger floor
For the near optimum root thickness of 2.3 m, a nearly fixed ratio between passenger floor area and total wing platform exists, which determines the minimum size of any vehicle.

Thickness-to-chord ratio
For a given lift coefficient, freestream mach number, and a limit on local Mach number, there will be a limit to the thickness-to-chord ratio for which we can design the wing. For a freestream Mach number of 0.6, a normal local Mach number of 1.2, and limitations on the pitching moment this thickness is about 16%. This result is discussed in more detail in chapter 3.

Lift-to-drag ratio
There will always be a lift-to-drag ratio poor enough to render a given range prohibitive. For the oblique flying wing and a range of 9000km this lift-to-drag ratio is near 6.5.

Fig. 2.3 Parametric study I

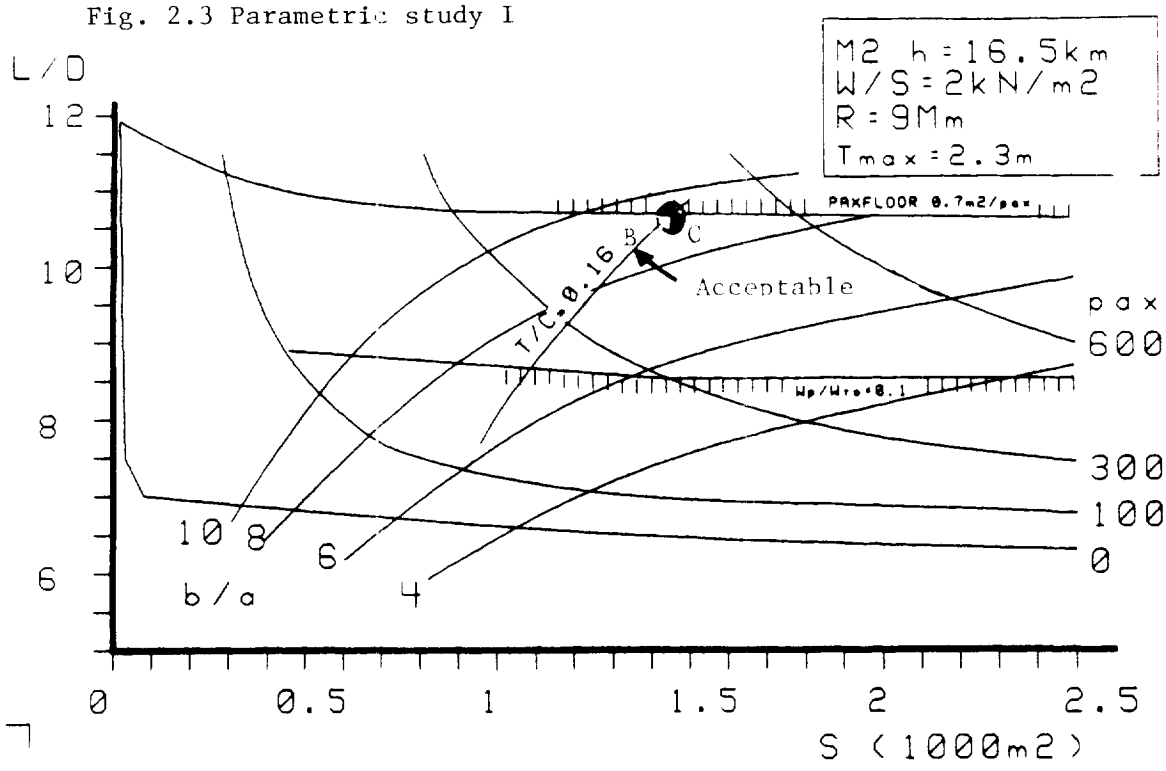

Fig. 2.4 Parametric study II

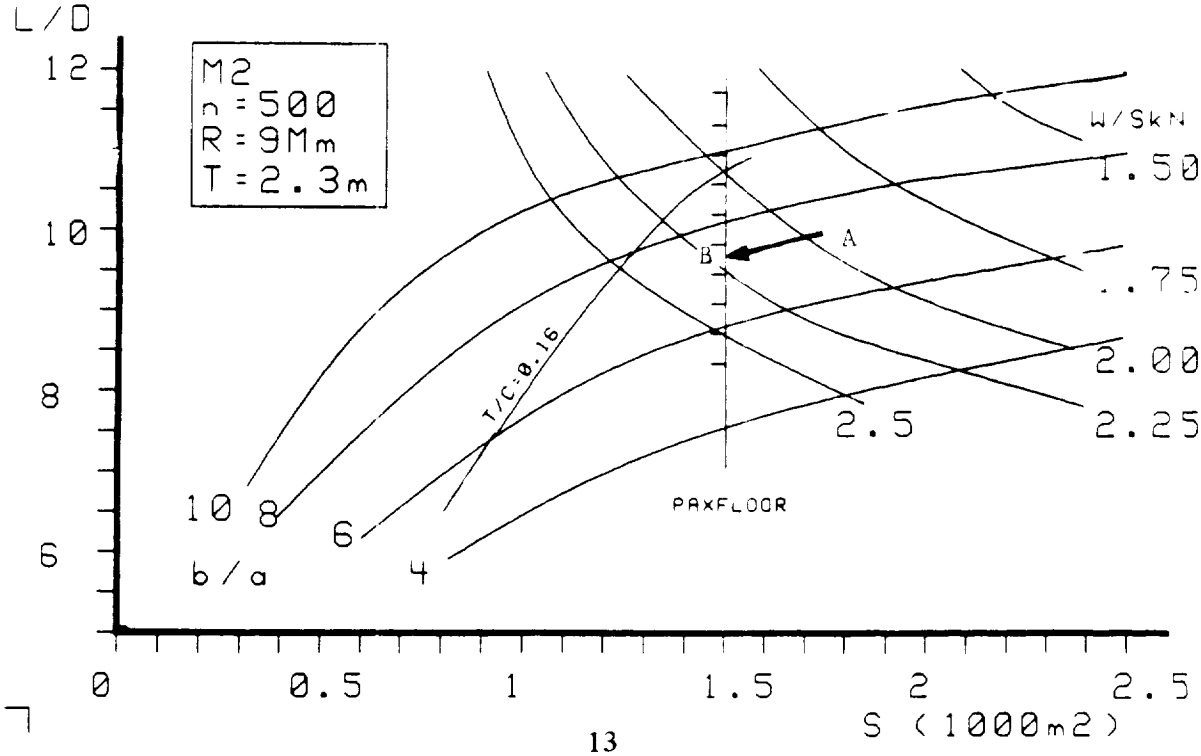

Fig. 2.3 shows the influence of size on the performance of Mach 2 oblique flying wings with the following parameters assumed constant :

altitude h=16.5 km	maximum thickness t_{max}=2.3
wingloading W/S= 2 kN/m^2	propulsive efficiency η=0.45

The lift-to-drag ratio was calculated as a function of the ellipse ratio and the wing planform area. The linearized expression for wing weight as presented in section 2.2, was used to find the required fuel weight and therefore the required lift-to-drag ratio to obtain the specified wing loading with a given payload.

Starting at point A in Fig. 2.3, an acceptable design, increasing the ellipse ratio with given payload is possible up to point B, where the maximum thickness constraint limits further reduction of the wing size. It is obvious that the smallest configuration with the highest payload fraction occurs at point C . This configuration accommodates 500 passengers. In this figure, lines of constant payload fraction are nearly horizontal. Increasing the lift-to-drag ratio by increasing the aspect ratio for a given payload will directly increase the payload fraction for a given altitude.

To be competitive, a new supersonic aircraft should have a payload fraction for this range which is similar to that of the B747. This means at least a payload fraction at least greater than 10%. A payload of 500 passengers constitutes an optimum since the payload fraction does not increase beyond this point, while the number of aircraft required by the market will go down.

For a given aspect ratio and aerodynamic refinement, the wing loading can be changed only by increasing range or by making the structure heavier (Fig. 2.4). Again we are bound by the minimum size aircraft constraint. If we start at A we can reduce the size of the vehicle until we are limited by the size of the passenger floor or the maximum section thickness. It is clear that the best configurations must employ very thick sections.

To obtain an economically competitive aircraft, the configuration should have a planform area between 800-1500m^2, aspect ratios between 8 and 12, and root thickness-to-chord ratios of at least 14%.

Fig. 2.5: Wave drag and induced drag of an oblique wing as a function of sweep angle and Mach number

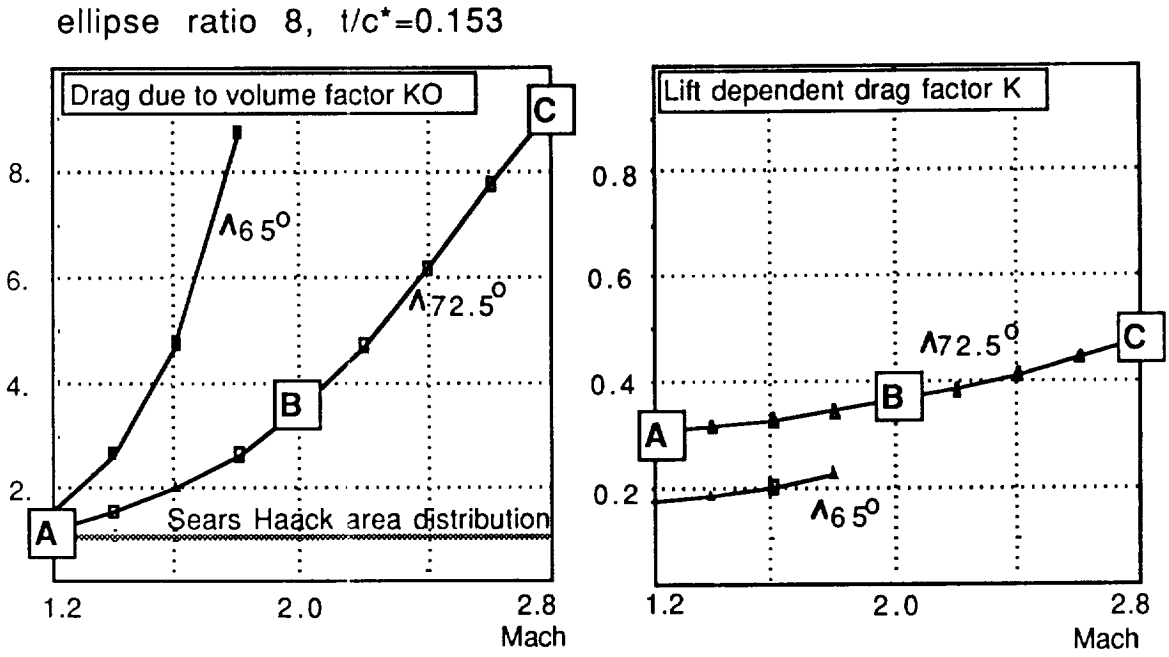

The wave drag of the wing is the average wave drag of the individual area distributions of its equivalent bodies for a full roll of the Mach-plane. The average wave drag at C is much higher than at A because the wave drag is quadratically related to the amplitude of the areadistribution.

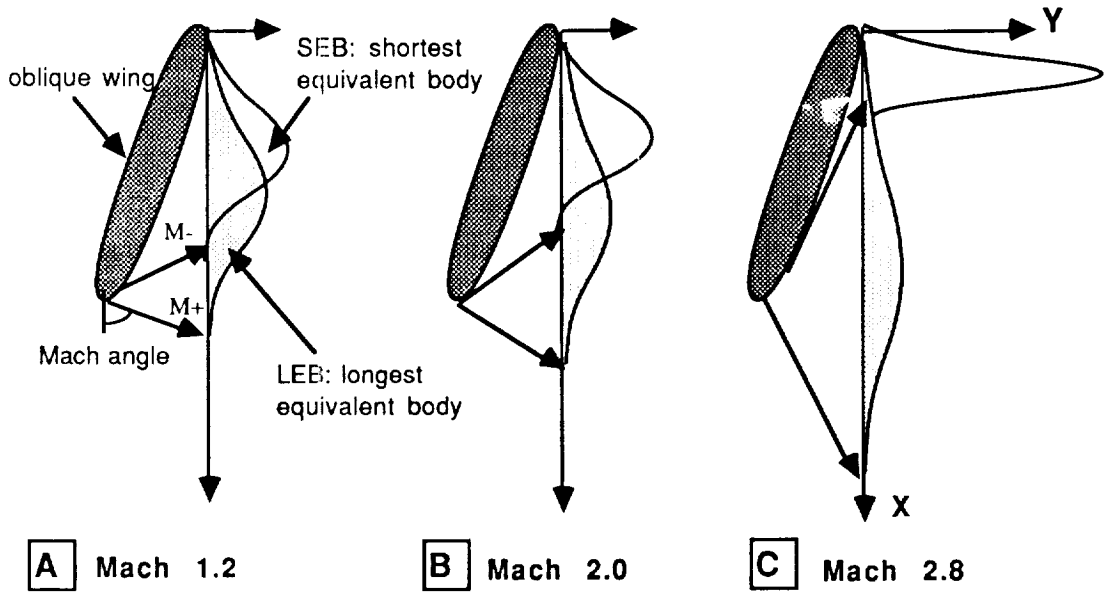

2.6 Effect of Cruise Mach number, Sweep and Altitude

In Fig. 2.5 the potential drag for the OFW is depicted as a function of wing sweep and Mach number. The factor KO represents the ratio of the volume-dependent wave drag to the Sears Haak area distribution wave drag. The factor K represents the lift-dependent drag. The total potential drag can now be expressed as

$$CD = KO\ CD_{Sears\ Haack} + K\ C_L^2$$

It is clear that in- or decreasing sweep by more than a few degrees from the optimum sweep angle results in very high drag penalties. The supersonic area rule, as presented by Robert T. Jones [19] and Harvard Lomax [22], provides us with an explanation. It states that the wave drag of a supersonic configuration is related to the average wave drag of all the equivalent supersonic bodies. The beginning and end of an equivalent supersonic body is determined by the intersection of a line along which pressure differences can travel [M+ to M-] and the body center line.

For a Mach number of 1 all equivalent bodies have the same length and the average wave drag of the wing is just the minimum, KO=1. Increasing the Mach number will increase the difference in length between the shortest equivalent body and the longest equivalent body. Since the wave drag is quadratically related to the amplitude of the area distribution, the average wave drag of the area distributions is much higher at Mach 2.8 than at Mach 1.2. Further increase of the Mach number will make the leading edge supersonic. For a supersonic leading edge, the equivalent body length associated with the M- lines will go to zero for an oblique wing of infinite aspect ratio. For an unswept aspect ratio of 10.2 the volume-dependent wave drag will be 25 times higher than the minimum value obtained at 90^o sweep.

Using the aerodynamic model of section 2.2, we can calculate the lift-to-drag ratio of the configuration as a function of Mach number and the Mach number normal to the average sweep angle. For each Mach number, a different wing normal Mach number gives the maximum value of lift-to-drag.

Mach<1.6	M_n=0.7
1.6<Mach<2.2	M_n=0.6
Mach>2.2	M_n=0.5

The sweep of the long axis of the ellipse can be found by taking the inverse cosine of the

Fig. 2.6: Effect of Mn Number on Lift-to-Drag ratio

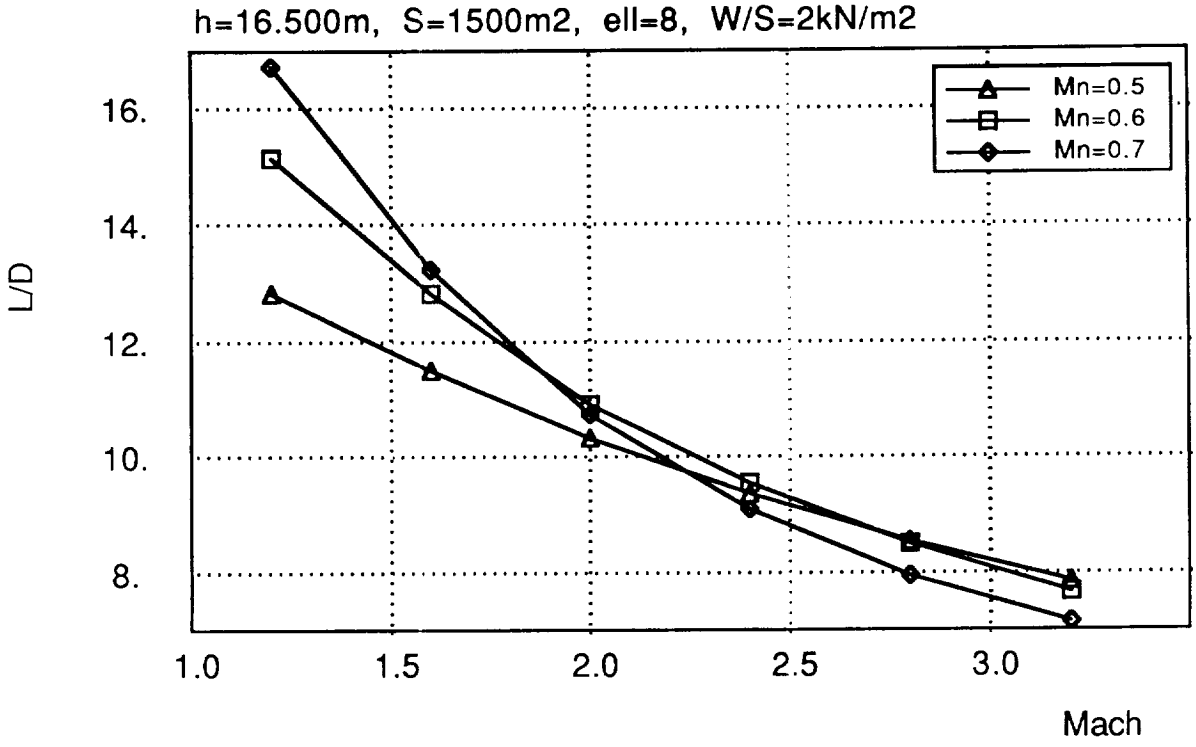

Fig. 2.7: Effect of Altitude and Payload fraction on Lift-to Drag ratio

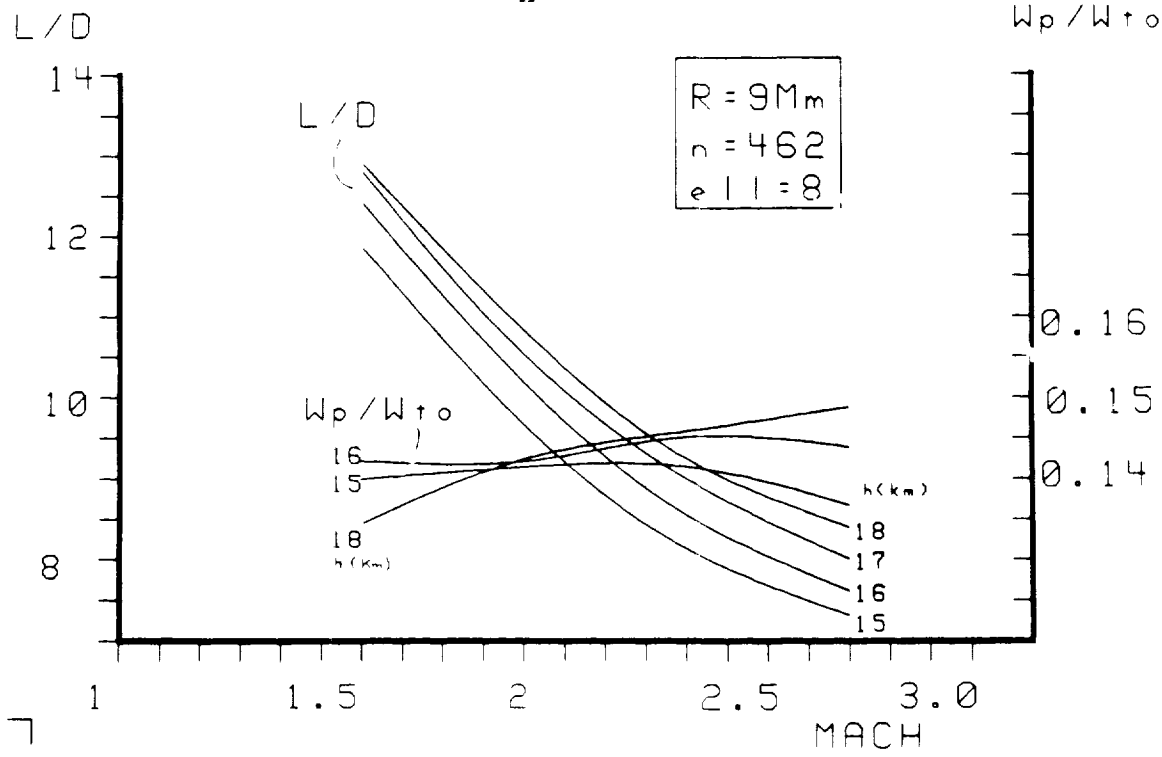

ratio of normal to freestream Mach number. It is clear from Fig. 2.6 that designing an airfoil for Mn=0.6 will result in good lift-to-drag ratios over the entire Mach range.

In Fig. 2.7 the lift-to-drag ratio and the payload fraction of the configuration with varying altitude are shown based on the full model described in 2.2. Even though the maximum lift-to-drag ratio is obtained for the highest altitude considered for every Mach number, an altitude of 16 km will result in near maximal payload fractions over the entire range of Mach numbers considered. Beyond 16.5 km the engine weight will increase almost as quickly with altitude as the fuel weight saved by the lift-to-drag ratio increase. [Note: 1]

From these considerations it follows that a $C_L M^2$ of 0.3 will be usable for any OFW cruising at Mach numbers between 1.5 and 2.8. Since we established in section 2.3 that for a given altitude, maximum lift-to-drag ratio and payload fraction are interchangeable we could use lift-to-drag ratio as the new objective function.

If we were to change the design range, the initial cruise wing loading and altitude would change, but, to first order, not the design lift coefficient. Kuchemann & Weber [10] as well as Torenbeek [15] have pointed out that the optimum ratio of the cruise lift coefficient and the lift coefficient at which the maximum lift-to-drag ratio is achieved remains constant for long range aircraft. Since increasing the range will mean taking on additional fuel with constant wing area the maximum lift-to-drag ratio will remain constant except for the influence of altitude on Reynolds number. The following chapters may therefore be applicable to any range between 6 Mm and 12 Mm.

Note:

[1] In a private communication Robert T. Jones disagreed with this statement.He agreed that one needs a greater engine diameter for flight at higher altitudes, but he argued that the loads on the engine didn't change so the weight of the engine shouldn't change either. The bigger engine should than be downrated for operation at lower altitudes.

3 DEVELOPMENT OF THE AIRFOIL

3.1 Objectives and Requirements

In the previous chapter we showed that an airfoil for which $C_L M^2 = 0.3$ and which has a thickness of at least 14% will give the configuration an economically competitive payload fraction.

The airfoil must be designed with a sufficiently small transonic wave drag. For current subsonic transports, a drag rise of 20 counts (0.002) is considered acceptable for the high-speed cruise condition. According to simple sweep theory, a 70^o swept wing with airfoils operating at this drag rise condition will have a total drag increase of only 1%.

The airfoil should be designed for Mach numbers between 0.5 and 0.7, to be used for the full range of OFW sweep angles and Mach numbers. We will attempt to reach this goal with just one airfoil-family design. In section 2.2 we mentioned that if control authority is provided by a narrow trailing edge flap, the location of the liftvector is limited to 32% of the chord.

Other considerations in the design were related to the utilization of the geometry by passengers. The relative thickness distribution over the chord was chosen to enable maximum use of the cabin Since passengers only accept very small inclinations of the cabin floor, the airfoil bottom was designed in such a way that for most of the operation the floor will be level. The airfoil section should also provide adequate space for the landing gear and systems.

3.2 Baseline Airfoil Design

We designed the airfoil for a Reynolds number of 200 million, and set the transition at 2% from the leading edge, to simulate the cruising conditions. For a two aisle layout the best utilization of the cabin is obtained with the maximum thickness at 35% of the chord.

At Mach 0.7, the upper surface normal Mach number distribution needs to be close to the maximum shockfree value over half the chord if we want a resultant lift vector at 32% of the chord. We found that an airfoil with a flat pressure distribution at Mach 0.7 had the same drag-rise $C_L M^2$ between Mach 0.5 and Mach 0.7.

The recovery was designed with Head's [17] turbulent boundary layer method. We defined the separation point at H=2.0. Low-speed airfoil designs will have the highest pressure gradients at the beginning of the recovery. But such steep gradients will change the location of the shock at the higher Mach numbers, and therefore the recovery has to start more gradually. The lower surface and the aft upper surface are then tailored to get the appropriate pitching moment and thickness.

The OW701014 [20] airfoil had the required flat supercritical pressure distribution at Mach 0.7. We therefore modified the pressure recovery of this airfoil to satisfy the pitching moment requirements, while leaving the first half of the upper pressure distribution undisturbed. These modifications were done with Panda, an interactive subsonic airfoil design program. After each modification, we analyzed the airfoil pressure distribution for Mach 0.5, 0.6 and 0.7 at the required lift with ARC2D. For most of this design phase a coarse grid (Fig. 3.1) was used since this enabled us to run jobs of less than 200 seconds on the Cray XMP. As can be seen, most of the grid points are in the boundary layer.

Fig. 3.2 shows the iso-Mach lines at the design condition of Mach 0.7. The rapid acceleration of the flow at the nose and the constant local Mach number of 1.2 on the rooftop are very notable. The waviness of the lines is caused by grid coarseness. It is also possible to look at the boundary layer velocity in more detail. Figs. 3.3a,b show the nondimensionalized velocity and Mach number across the boundary layer during the recovery. The flow is fully attached and the boundary layer is very thin.

Figs. 3.4a,b,c,d show the 16% OFW airfoil pressure distribution at the drag divergence lift coefficient for Mach 0.50, 0.6, 0.65 and 0.7. For all of these Mach numbers, the required trimmed lift was just obtained with the present baseline design. One can clearly observe the shock travelling from the leading to the trailing edge as the Mach number increases.

Figs. 3.5 a,b,c show the characteristics of the airfoil design according to ARC2D. We have also included results from an analysis done with the BAUER-code. The BAUER code predicts significantly less drag than the ARC2D code. However, once the ARC2D grid is refined five-fold, the drag of the section decreases by 30 counts and the predicted drags are very close. The pressure distribution, and therefore the pitching moment and lift characteristics, remained unchanged by the grid refinement.

Fig. 3.1 GRID

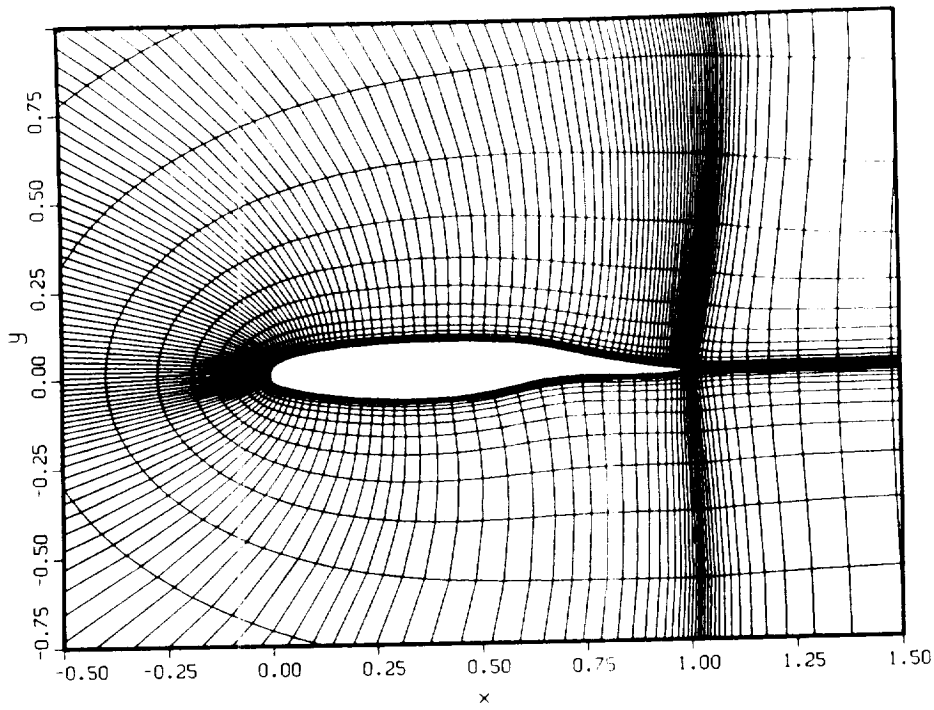

Fig. 3.2: Lines of Constant Mach Number

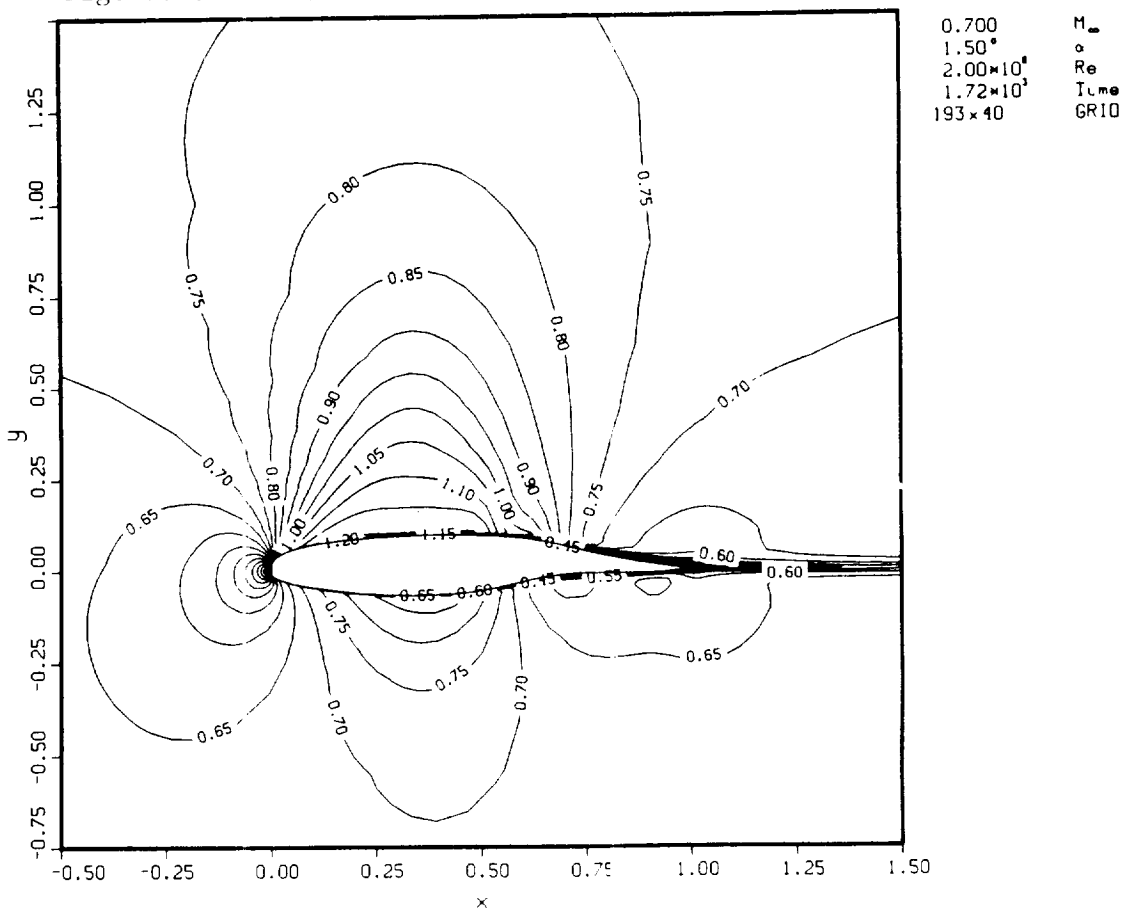

Fig. 3.3a VELOCITY

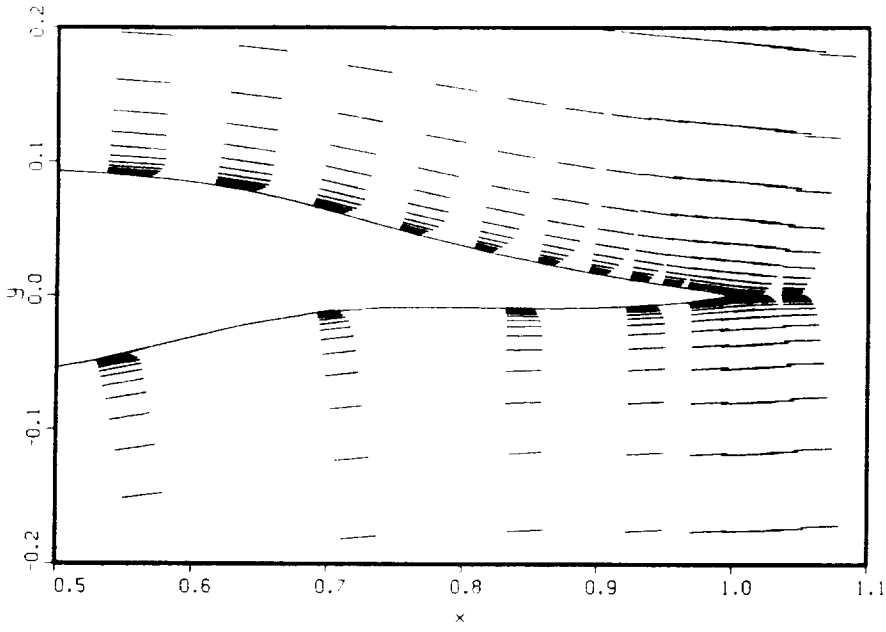

Fig. 3.3b MACH NUMBER

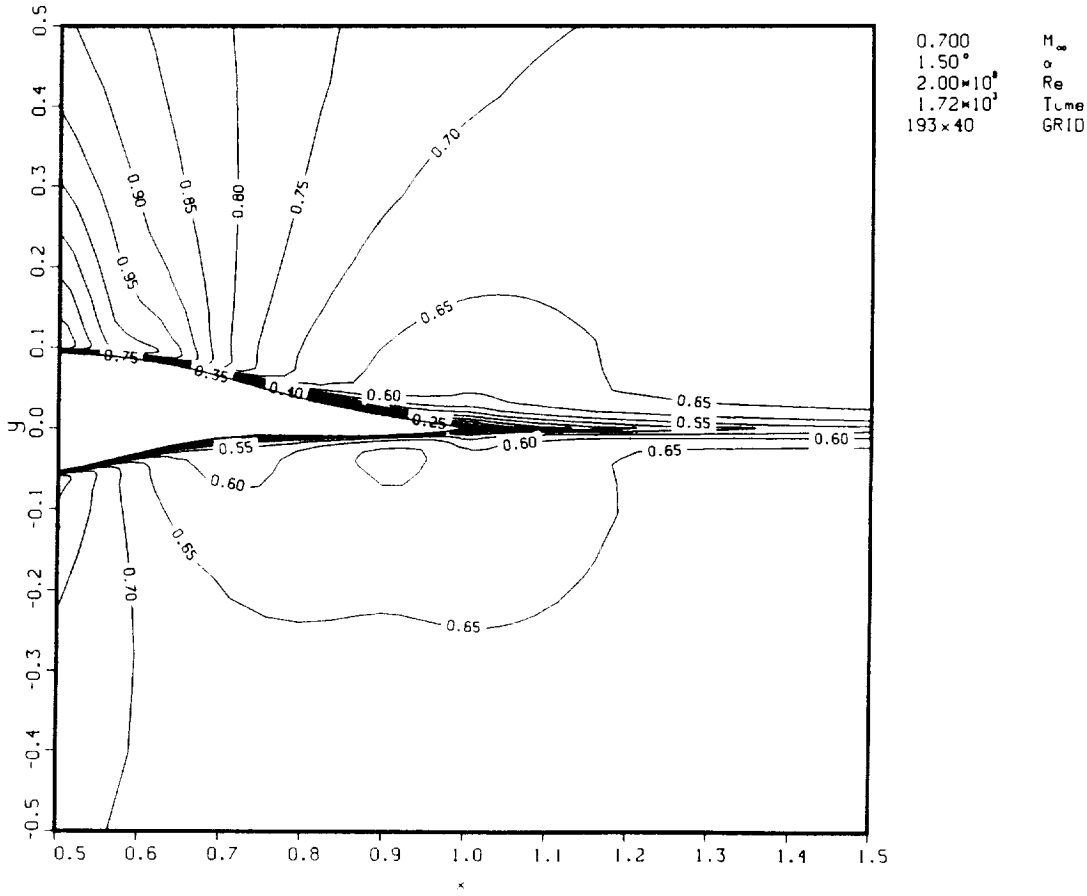

Fig. 3.4a OFWA16 Pressure Distribution

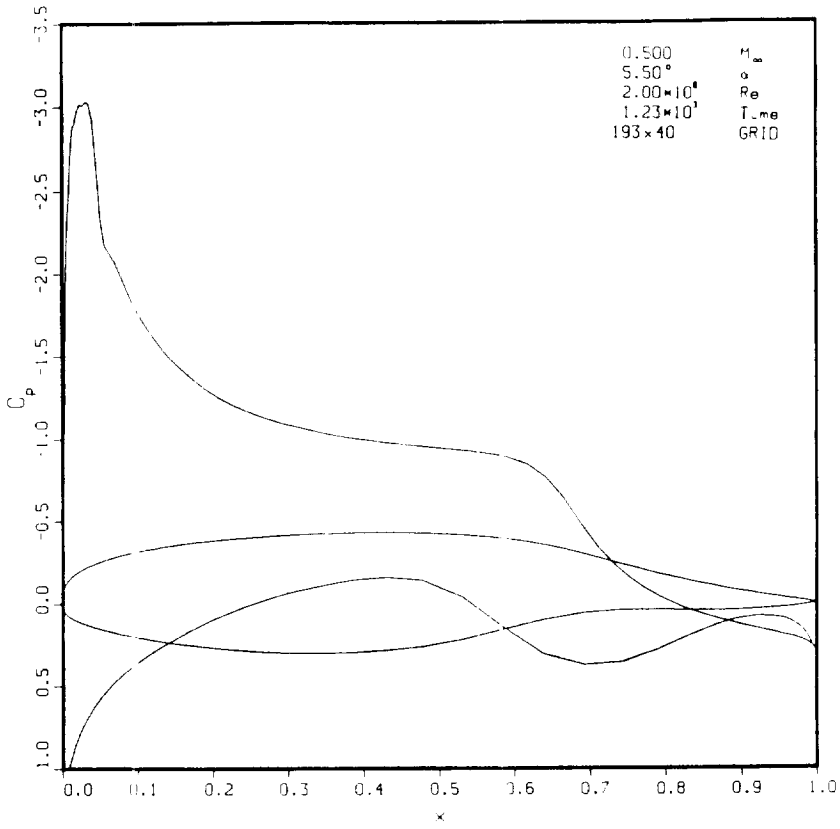

Fig. 3.4b

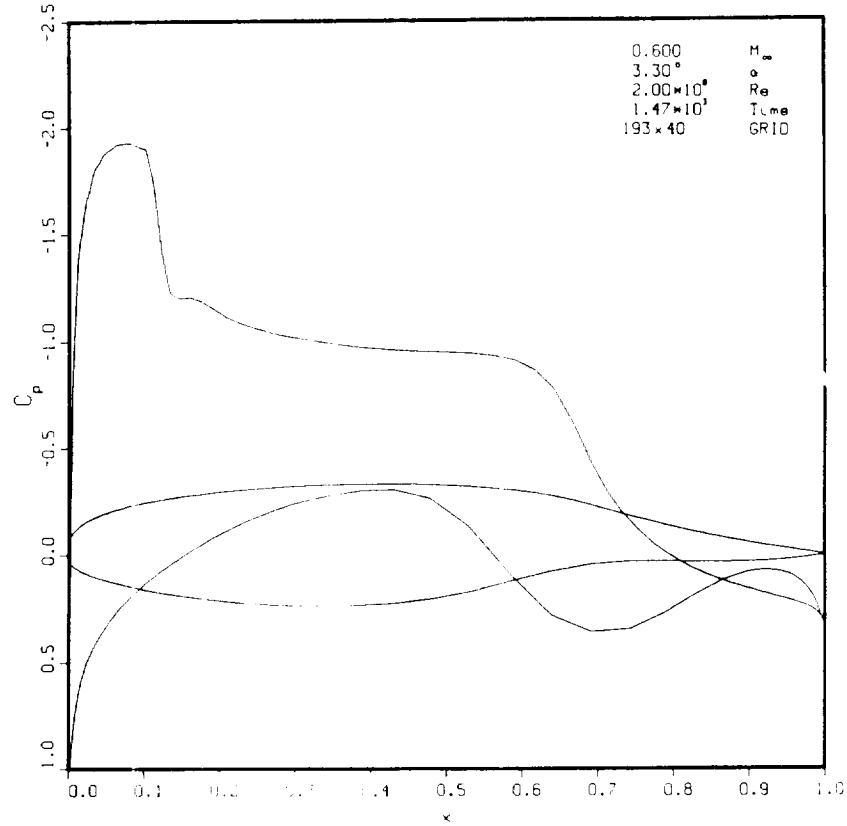

Fig. 3.4c

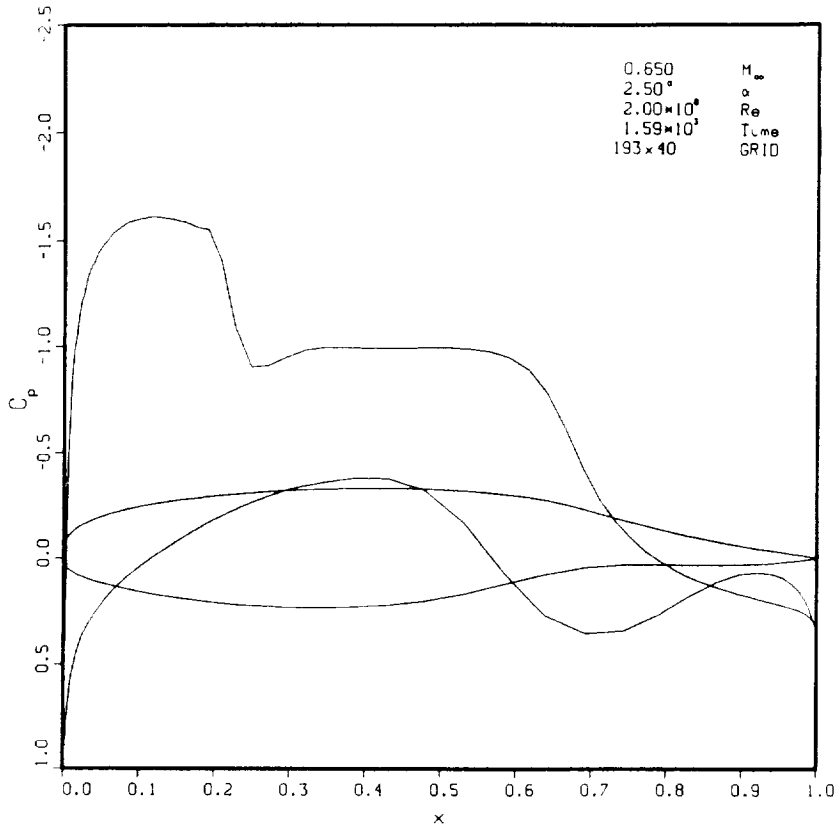

Fig. 3.4d

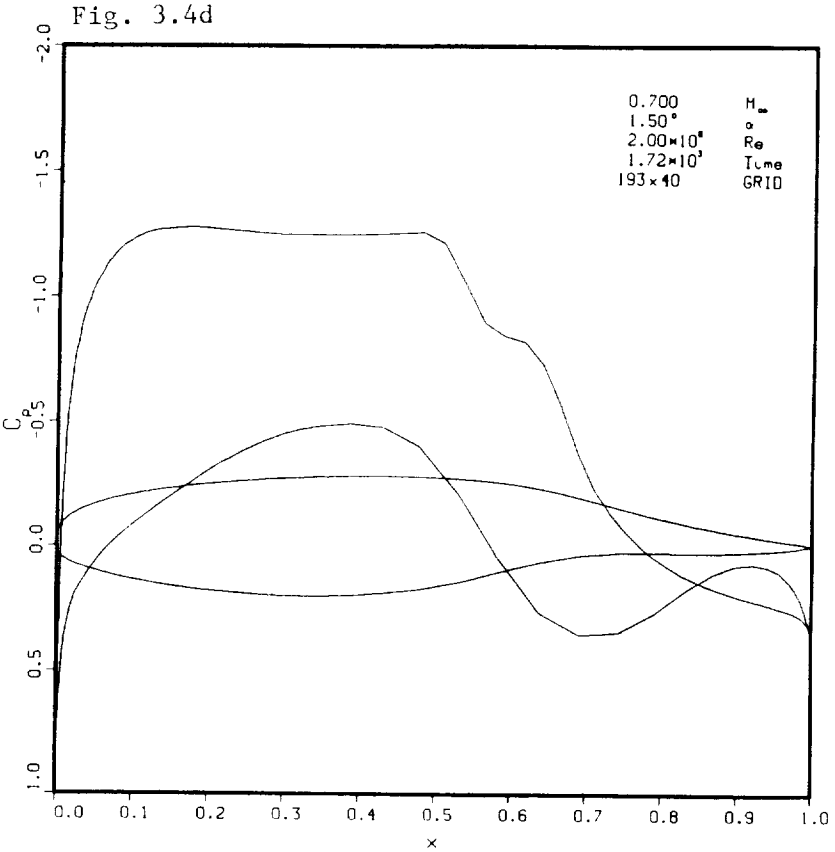

Fig. 3.4e

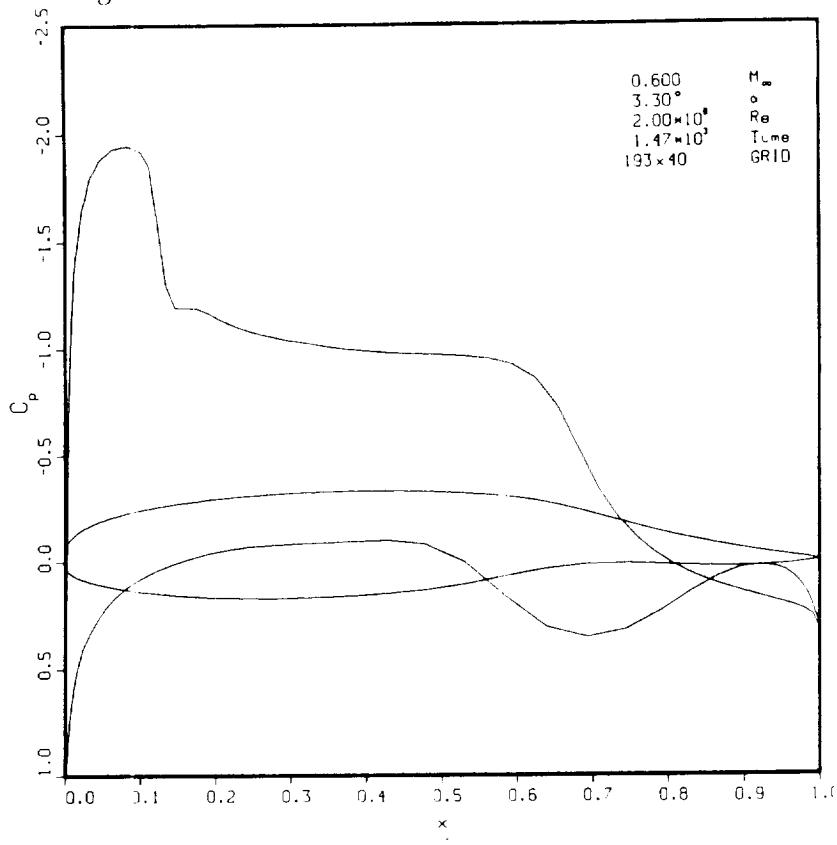

Fig. 3.4f

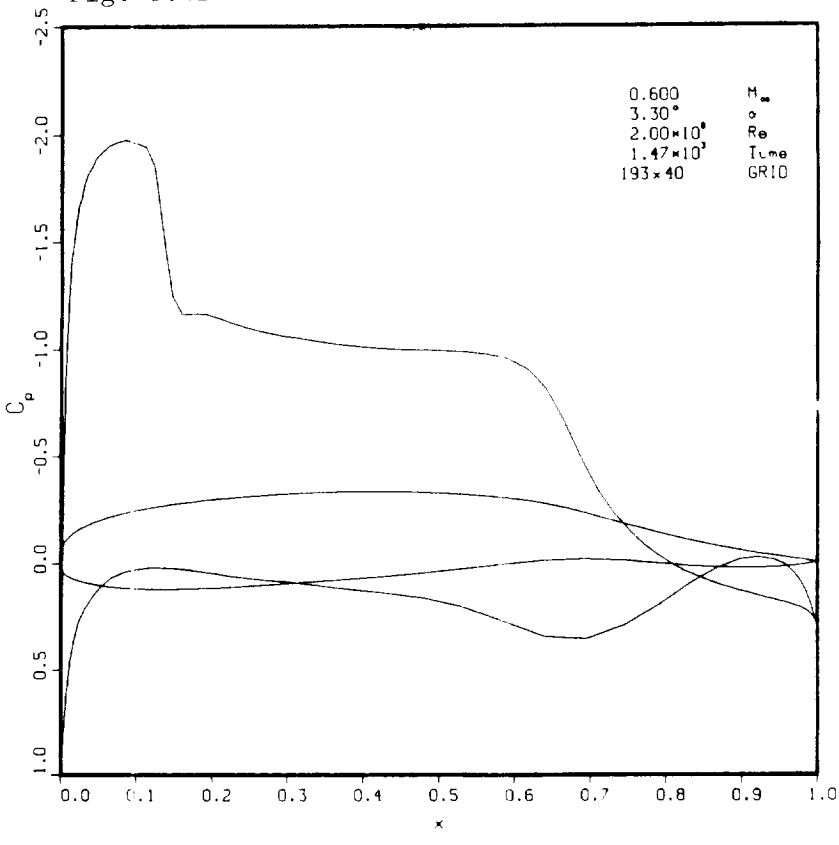

Fig. 3.5: Characteristics of 16% OFW airfoil
Re 2e8, transition at 2% chord, 193x40 grid

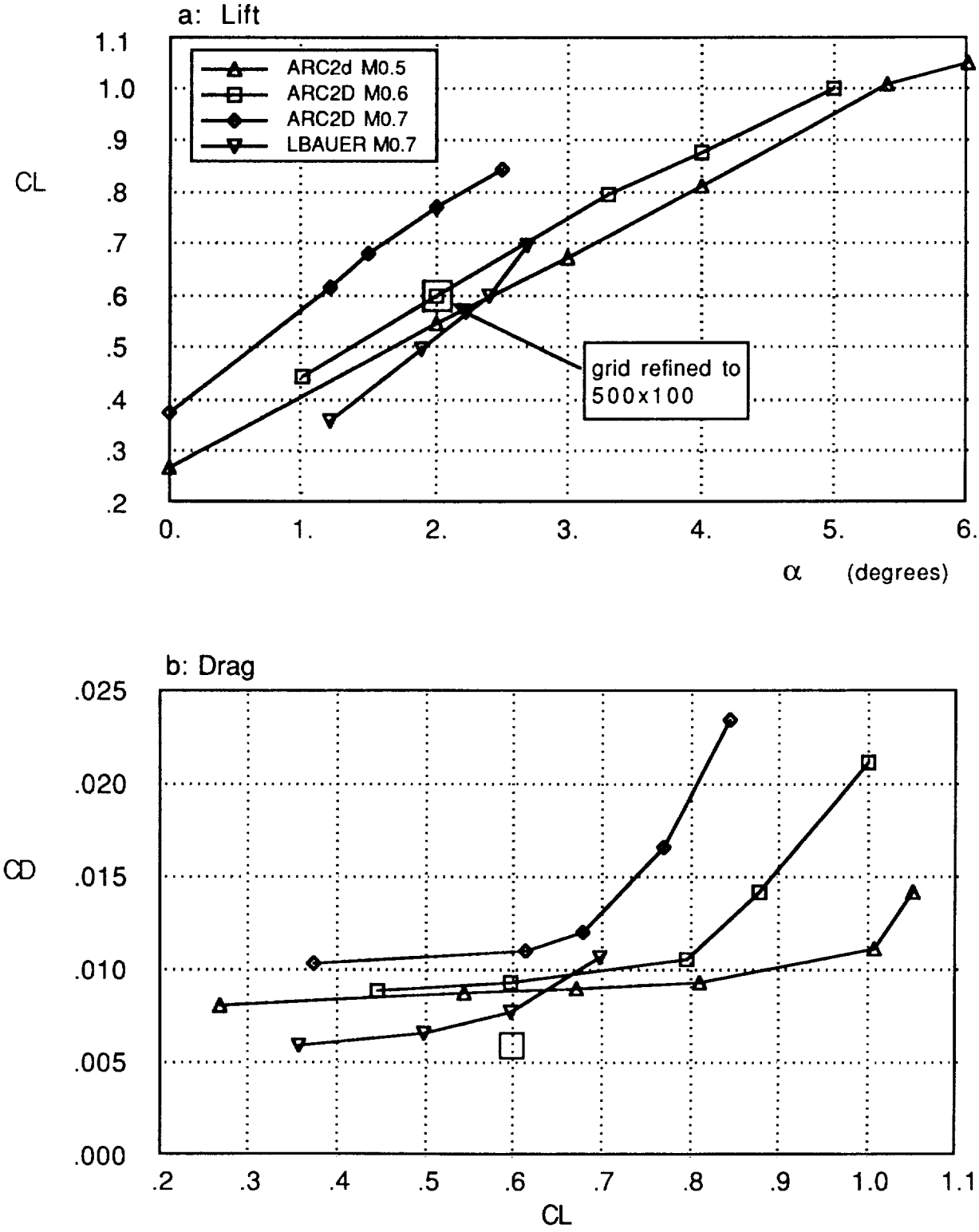

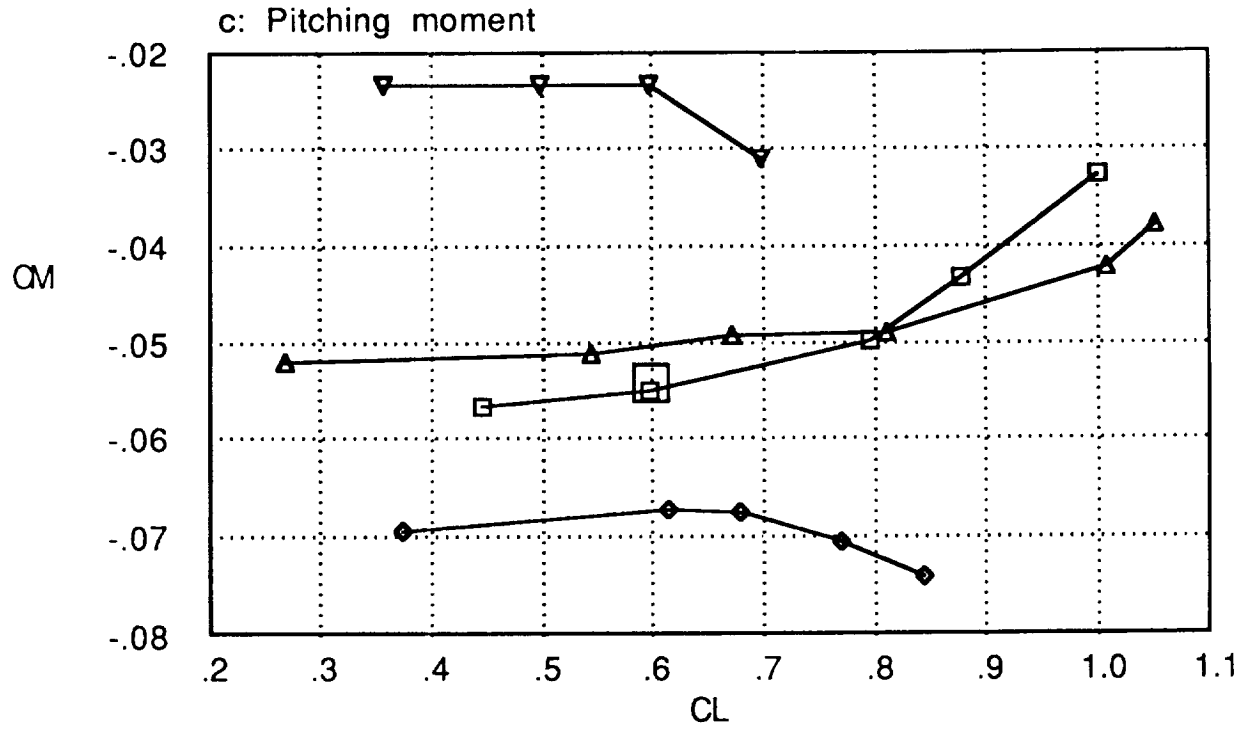

Fig. 3.6: OFW family of airfoils

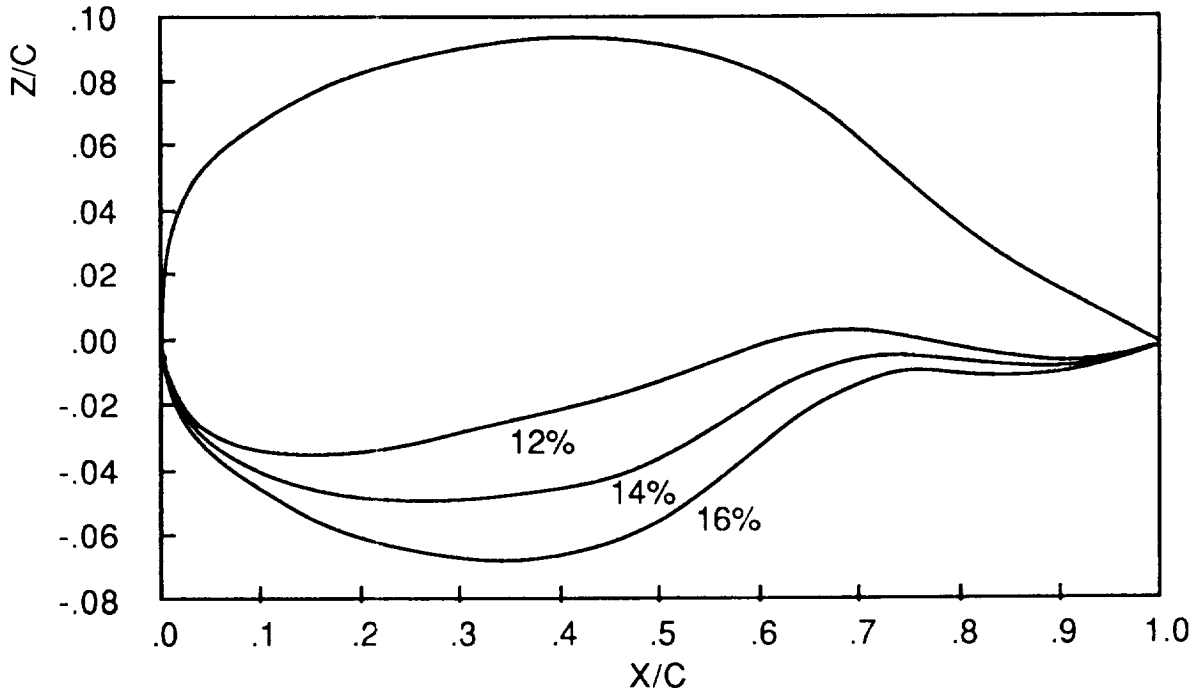

3.3 Thickness Trade-off

After the baseline t/c=16% airfoil was designed, it was possible to design a family of airfoils with the same pitching moment characteristics but different thicknesses. Since the upper surface of the airfoil is already designed close to the optimum, only the lower surface remains as a variable. In addition, in order not to disturb the flow on the upper surface we had to maintain the lower surface leading and trailing edge geometry.

Airfoils of this kind can be obtained by adding or subtracting a thickness distribution represented by a transformed sine function over a 0 to π range. The added thickness distribution is zero on the trailing and leading edge and reaches a maximum at 40% of the chord. Adding this thickness distribution to the lower surface did not change the location of the center of pressure. These airfoils are shown in Fig.3.6. Instead of referring to them by their actual thickness t/c we use t/c*,.which is defined as 1.5 times the section volume parameter ($=^{area}/_{t\ c}$). This variable has more physical significance than t/c if we want to relate the achievable lift to the section thickness.

Figs. 3.4 e, f show the 12% and the 14% thick airfoils with their pressure distributions at α=3.3° and M 0.6. In Fig. 3.7 and 3.8 one can see the lift, drag and pitching moment of these airfoils for the drag-rise condition, with and without trim. We trimmed the airfoil with a 10% narrow trailing edge flap. As expected, lift is lost when thickness is increased. Since we know the drag-rise characteristics of the airfoil and the C_L at which drag-rise occurs for each airfoil, we can now model drag-rise in the aircraft polar.

To select the best maximum thickness for our configuration, we express the change in takeoff weight relative to the baseline configuration (point C in Fig. 2.3) as a function of the maximum thickness-to-chord ratio. The size of the passenger cabin and the takeoff weight are fixed.The maximum thickness ratio influences the takeoff weight because it

1) changes the planform area required to accommodate the passengers, and this area determines the structural weight fraction, and
2) changes the lift-to-drag ratio, and this ratio determines the fuel weight fraction.

The lift and drag coefficient at the drag-divergence condition can be expressed as:

$$CL_{dd}=CL_{dd,2D}\cos^2\Lambda$$

$$CD_{dd}=(CD_{parasite,ref}-CD_{wave,ref})+CD_{wave,ref}\left[\frac{t/c^*}{t/c^*_{ref}}\right]+K\,CL_{dd}^2$$

where:

$CL_{dd,2D}$	Drag diverergence CL for varying t/c* from Fig. 3.7
$CD_{parasite,ref}$-$CD_{wave,ref}$	0.00413 from Ref. 41
$CD_{wave,ref}$	0.00133 from Ref. 41 or Section 2.2
K	0.370 from Ref. 41 or Section 2.2

The required ratio of planform area to reference planform area for a constant cabin floor area follows from the relation in Fig. 2.1. For a given ellipse ratio this corresponds to a certain t/c* which, in turn, can be converted to a lift-to-drag ratio by the previous relations. The fuel weight fraction can be calculated with the Brequet equation. The change in planform area will also influence a fraction of the structural weight. If we assume a constant total weight and a varying payload fraction, the structural weight fraction that depends on the wing area will vary linearly with the planform area. For a constant total weight the powerplant weight fraction will increase linearly with drag and inversely with ambient density:

$$\left[\frac{Wpp}{Wto}\right] = \left(\frac{Wpp_{ref}}{Wto_{ref}} \frac{\rho_{ref}}{\rho} \frac{CL_{ref}}{CD_{ref}} \frac{CD}{CL}\right) = \left(\frac{Wpp_{ref}}{Wto_{ref}} \frac{CD\ S}{CD_{ref} S_{ref}}\right)$$

The combined effect on the weight fractions due to variation of the thickness ratio is shown in the last column of table 3.3.1. As observed before qualitatively, the best root thickness-to-chord ratio is around t/c*=0.153. Serious penalties can be expected for deviations of more than 10% from this value.

table 3.3.1: Structural and Fuel Weight Fraction as a Function of Thickness Ratio

[tmax]	$\left[\frac{S}{Sref}\right]=\left[\frac{Spref}{Sp}\right]$	$\left[t/c^*\right]$	$\left[L/D\right]_{DD}$	$\left[\frac{Wf}{Wto}\right]$	$\left[\frac{Ws}{Wto}\right]$	$\left[\frac{Wpp}{Wto}\right]$	$\left[\frac{Ws+Wf+Wpp}{W_o}\right]$
2.1	1.81	0.104	11.6	0.38	0.33	0.19	0.91
2.2	1.24	0.132	10.7	0.41	0.22	0.12	0.76
2.3,ref	1.00	0.153	9.89	0.43	0.18	0.10	0.72
2.4	0.92	0.166	9.29	0.46	0.17	0.09	0.72
2.5	0.85	0.195	7.82	0.51	0.15	0.09	0.76
2.7	0.73	0.229	6.01	0.62	0.13	0.08	0.83

Fig. 3.7: Thickness tradeoff

ΔCD=0.002 and trim @ 0.32c

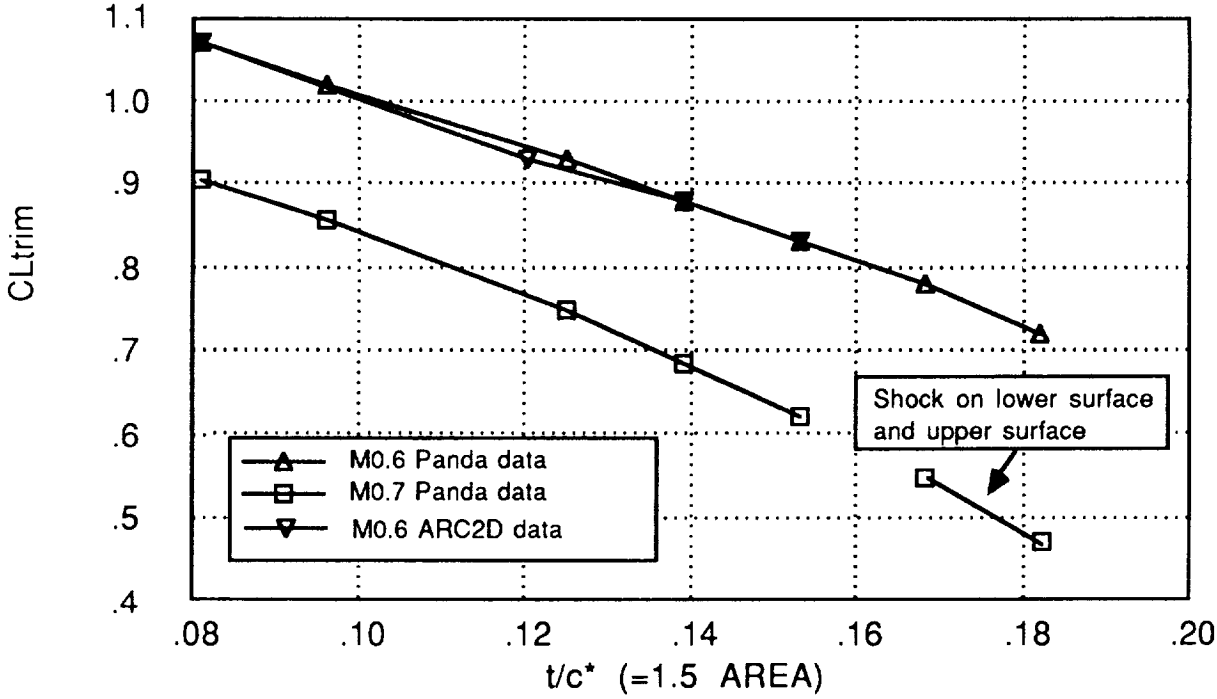

Fig. 3.8: Airfoils analyzed with ARC2D

M0.6, alpha=3.3, grid:193x40

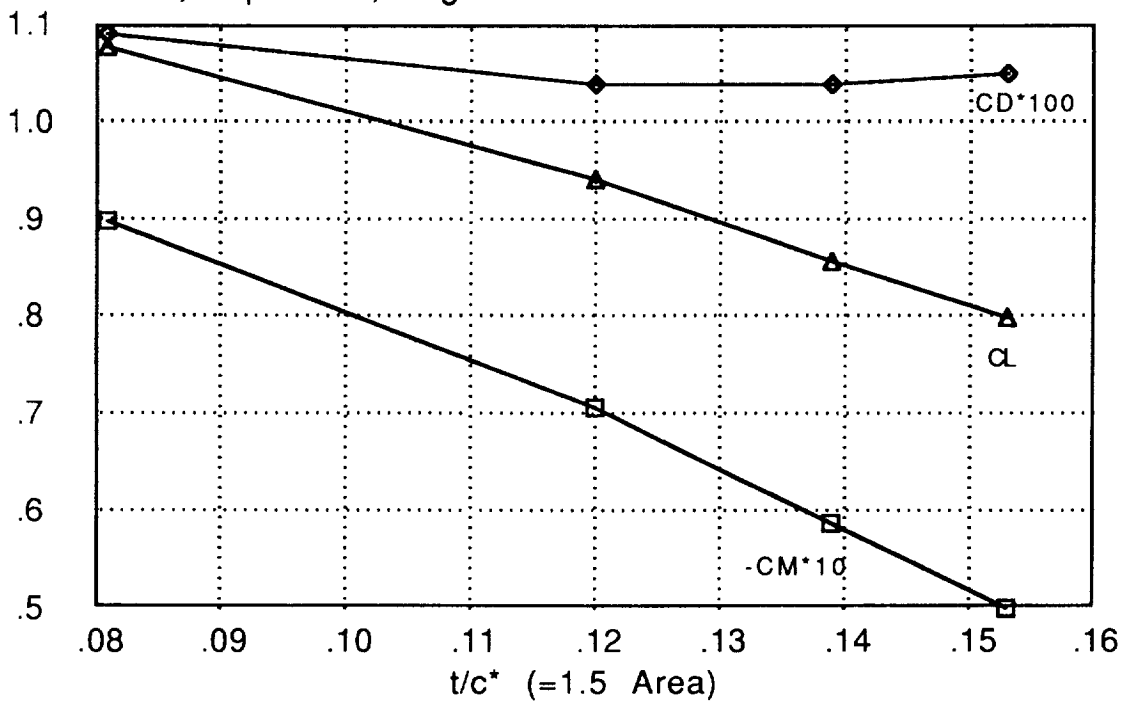

4 THREE DIMENSIONAL WING DESIGN

4.1 General considerations

The following considerations play an important role in the determination of an acceptable pressure distribution on the Oblique Flying Wing:

1. The wing has to provide sufficient resultant lift at 32% chord location. This can be achieved by scaling the airfoil pressure distributions with simple sweep theory.

2. The loading of the wing should be nearly elliptic in both the y- and x-projection to minimize the induced drag of a supersonic oblique wing. It can be shown that for a high (unswept) aspect ratio oblique wing, the loading is near-elliptic in the x-projection when it is elliptic in the y-projection [2].

3. A Sears-Haack area distribution minimizes the volume-dependent wave drag of the wing [3, 48].

4. In the design of the airfoil we used a Navier-Stokes code. This code models shocks and shock-induced flow separation. We designed the airfoils in such a way that shocks gradually move to the tailing edge and gradually increase in strength with increases in angle of attack. The linear theory that is used to design the three-dimensional wing does not model these non-linear effects, but if the wing has the same transonic local normal Mach numbers distribution as the airfoils, we can expect it to have similar non-linear behavior.

5. To prove that the three-dimensional wing is separation free we would have to do a three dimensional boundary layer analysis. In the absence of this analysis we should at least show that the flow has a positive velocity in the direction normal to the isobars.

6. The prescribed pressure distribution should result in a geometrically realizable wing. It is for this reason that we propose to specify the thickness distribution and warp the mean camber surface of the wing to satisfy all other requirements.

4.2 Wing Planform and Basic Thickness Distribution

We find the wing planform and the airfoil selection along the wing span from the following

considerations:

a) A minimim size wing without excessive drag is obtained if the drag divergence lift coefficient $C_{L,dd}(t/c^*)$ is achieved over the whole wingspan (Fig. 3.7).

b) A wing with minimum induced drag is obtained with elliptic loading. For a given $C_L(t/c^*)c$ at the root we can find the C_Lc at a given spanwise location y.

c) A wing with minimum volume-dependent drag is obtained with a Sears Haack area distribution. For a given $A(y)= \frac{2}{3}[\, c^2\, t/c^*]$ at the root we can find the A(y) at a given spanwise location y

If we select a root $t/c^*=0.153$, as suggested by the analysis in section 3.3, we know the distribution of $C_{L,dd}c$ and A over the span. We now have two known quantities (i.e. $C_{L,dd}$ and A) and we have to solve for the two unknows $t/c^*(y)$ and c(y).

In Fig. 4.1 the spanwise distribution of chord, thickness-to-chord ratio and local lift coefficient are depicted for a wing with a Sears Haack area distribution and elliptic loading with OFW-airfoils. The wing planform resembles an ellipse, but is slightly more tapered. The higher taper ratio, and therefore decreased wetted area, is possible because the airfoils become thinner near the tips. Thinner airfoils have higher lift coefficients, so less chord is required to carry a given load.

To simplify the manufacturing the wing consists of a limited number of linearly tapered sections instead of a continually curved leading and trailing edge. It is clear that deviation from the ideal area-distribution will result in extra volume-dependent wave drag. However, such small deviations from the elliptic loading will not cause significant additional induced drag.

To evaluate the trade-off between the number of linearly tapered sections and the drag we wrote a program to calculate of volume-dependent wave-drag of area distributions based on the Eminiton-Lord method [21]. This analysis showed that the wave drag of a linearly tapered oblique wing is almost twice that of a Sears Haack body. This would mean a decrease of 18% in lift-to-drag ratio of the OFW. Even the absolute wave drag of a linearly tapered wing was a third higher than that of a Sears-Haak area distribution although the volume was less. With the OFW wing design presented in Fig. 4.2 we obtained a wave drag that was no more than 13% higher than the theoretical minimum ($\Delta L/D=2\%$).

Fig. 4.1: Wing design on the basis of the airfoils

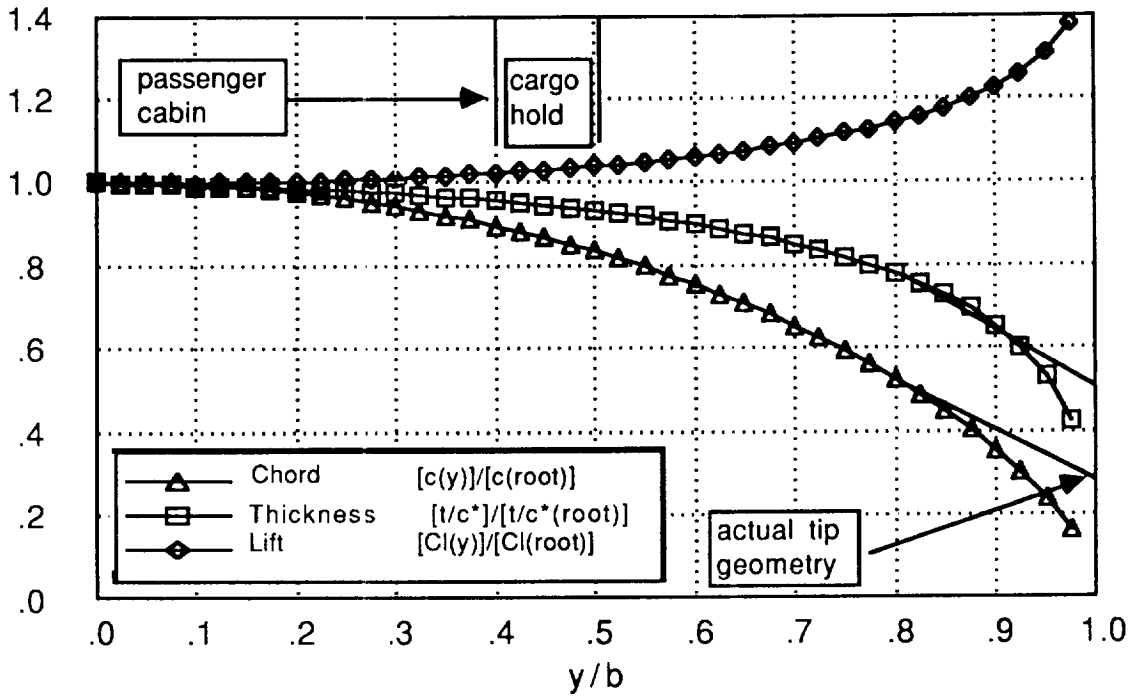

Fig. 4.2: OFW planform and thickness distribution

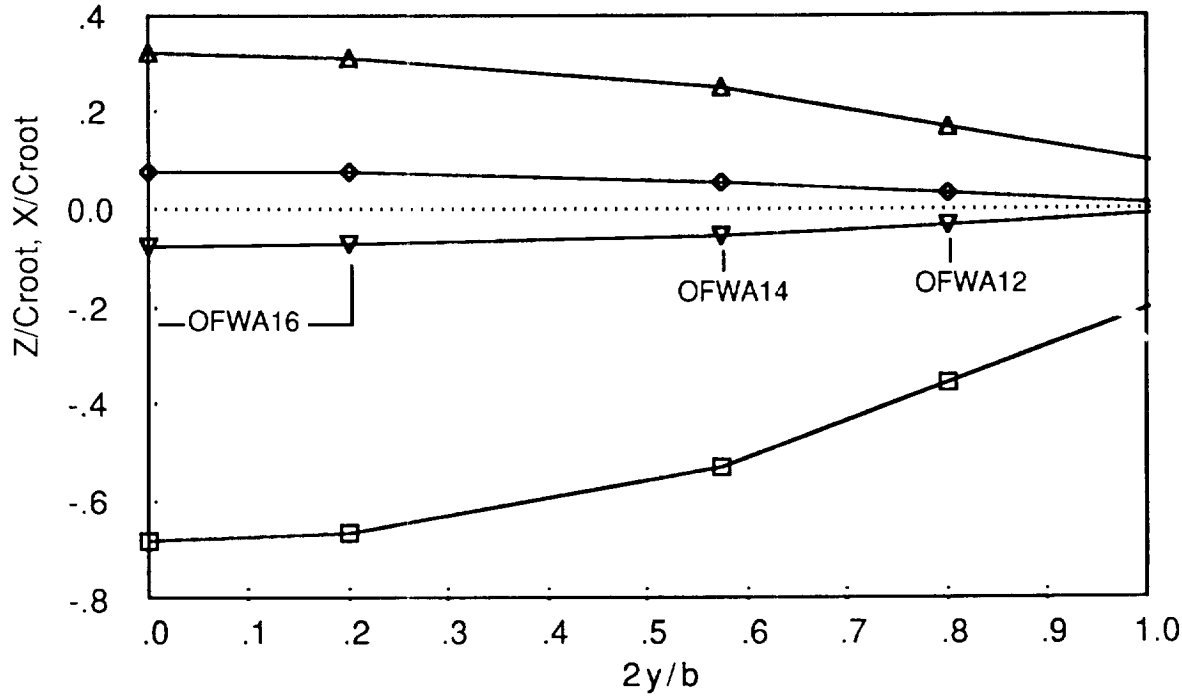

4.3 From a Two-Dimensional Pressure Distribution to a Three-Dimensional Wing

Introduction

In the 1960's Lock [23] developed techniques to transfer the pressure distribution from an airfoil to a wing based on local normal Mach number. He pointed out that the major disadvantage of the transformation lies in the fact that the magnitude of the velocity determines the local C_p, but its direction determines the local normal Mach number. Therefore, this transformation can only be made if one assumes that the local velocity has the same direction as the freestream velocity. This assumption is incorrect for low-aspect ratio wings as well as near the tips of high-aspect ratio wings. Another disadvantage is that if the upper surface pressures are determined by the airfoil normal Mach number distribution, the lower surface pressures, and therefore the loading ($C_{p,lower}$-$C_{p,upper}$), are determined by the thickness distribution. To control the loading, the thickness distribution has to be changed which may result in unrealizable geometries. This is probably the reason that simple sweep theory is often used to transfer pressure distribution from airfoil sections to the wing. Simple sweep theory relates the wing pressures to those of the airfoil with the following expression:

$$C_{p,3D} = C_{p,2D} \cos^2 \Lambda_{ref}$$

Instead of using the angle between the quarter chord line and the Y-axis as the reference sweep angle, Boppe [36] proposes using the angle between the line of two-dimensional shock locations projected on the wing and the Y-axis (see Fig. 2). Although this will assure a correct transformation based on normal local Mach number near this line, the transformation is incorrect for other locations and, in some cases, the shock may well appear elsewhere.

Boppe used an inverse panel code to find the slopes of the wing camber surface after he determined the desired pressure distribution based on simple sweep theory. It could be argued that with a non-linear inverse design code such as Boeing's A555 [38], a wing with any thickness and pressure distribution can be designed. There are however two major disadvantages in using non-linear inverse codes. First, they require more storage and speed than a linear potential code. Another disadvantage is that the perturbations due to thickness and camber can no longer be added, depriving us of a powerful tool in wing design. We will show that it is possible to use this linearity to determine the pressure distribution for a low-drag, geometrically-realizable wing.

Overview

Unlike previous method, the present method accounts for the influence of local taper, local sweep and three-dimensional induced velocities to specify the wing pressure distribution based on airfoil data. In an iterative way, the pressure distribution is calculated from the potential flow velocity perturbations for a given thickness distribution and the prescribed vorticity. The present method combines the philosophy of Lock's and Boppe's method to prescribe the vorticity on the wing. The vorticity in *supercritical* wing regions is based on airfoil transonic normal Mach numbers and includes the influence of local sweep and three-dimensional induced velocities, so that the appearance and the strength of the shock waves can be expected to resemble those of the airfoil. The vorticity in *subcritical* wing regions is scaled first with simple sweep theory, and then to achieve the desired load distribution.

Fig. 4.3 presents the computational algorithm. The airfoils, which were designed with a Navier-Stokes code [24], were analyzed with the potential flow code that was used for the three-dimensional wing geometry, at the same Mach number and angle of attack. The vorticity and the local normal Mach number predicted by the potential flow code were used to specify the vorticity (u_{vort}) distribution on the wing. In turn, the vorticity distribution is used to solve for the wing's camber with an inverse panel code. The induced velocity perturbations of this cambered wing are used in the next iteration.

Like those mentioned in the introduction, this method does not include a three-dimensional boundary layer analysis. Such an analysis is required if we want to check for flow separation. In the absence of such an analysis we would at least have to show that there is a positive velocity in the direction normal to the isobars according to potential flow. If a three-dimensional boundary layer analysis shows separation, the effective boundary layer may be added to the geometry and the present method repeated. If the separation occurs because the induced velocities increase the adverse pressure gradients relative to the airfoil's, the airfoil pressure recovery must be redesigned.

Detailed Description

From the arguments mentioned in the introduction it follows that specifying the vorticity distribution based on local normal Mach number will generally not result in a wing that has the desired load distribution. On the other hand, if one specifies the vorticity based on simple sweep theory one cannot control the location of the shocks, and the non-linear pressure distribution may look very different from the linear pressure distribution.

Fig. 4.3: Determination of the wing camber distribution

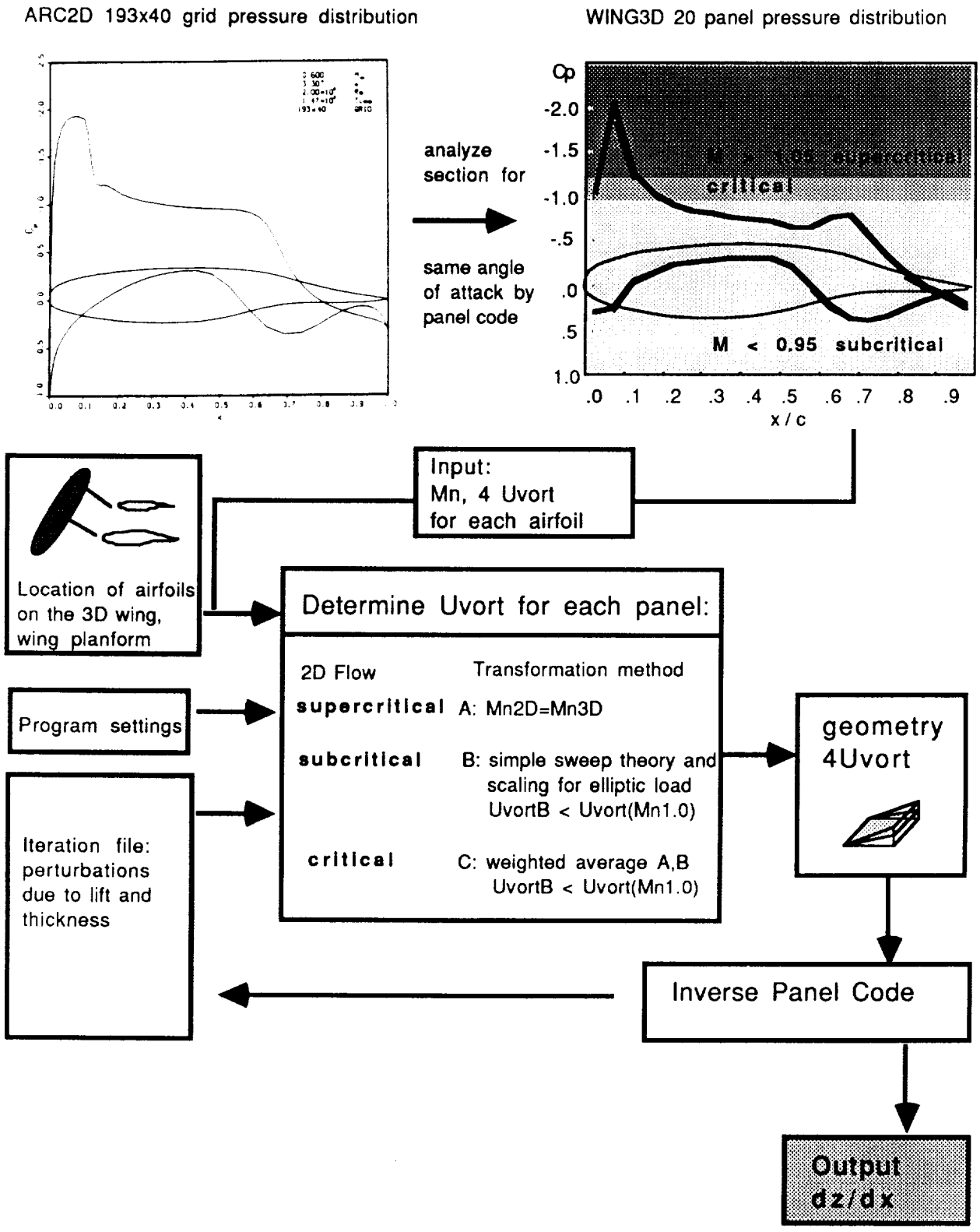

We therefore propose to use different criteria for different parts of the wing:

To satisfy the loading constraints we scale the vorticity of wing regions with subcritical pressures based on simple sweep theory. To obtain elliptic loading on the wing, it may be necessary to scale this distribution again with a correction factor $\lambda(y)$. To avoid the occurrence of shocks and separation the local normal Mach number should be limited to positive subsonic values:

$$u_{vort,3D} = \lambda\, u_{vort,2D} \cos^2\Lambda_{ref} \quad \text{but;} \quad u_{vort,3D}\,(M_n=0.0) < u_{vort,3D} < u_{vort,3D}\,(M_n=1.0)$$

If the transonic normal Mach numbers of the wing are the same as the corresponding airfoil Mach numbers, the non-linear effects on the three-dimensional wing will correspond approximately to those of the airfoil. Therefore it is sufficient to transfer only the supercritical pressures with the local normal Mach number criterion:

$$M_{l,n,3D} = \frac{Un_{3D}}{a_{3D}} = M_{2D.}$$

Using second-order small perturbation theory, we can write expressions for the local normal velocity and the local speed of sound to obtain the local normal Mach number. All the velocities are normalized with the freestream velocity:

Local normal velocity	$U_{n,3D} = \sqrt{\{(1+u)\cos\Lambda+v\sin\Lambda\}^2+w^2}$
Local velocity	$U_l = \sqrt{(1+u)^2+v^2+w^2}$
Local velocity of sound [30]	$a = \sqrt{1/M^2+\frac{1}{2}(\gamma-1)(1-U_l^2)}$.

In these expressions:

	M is	the freestream Mach number,
	Λ is	the panel quarter chord sweep angle, and
	u,w,v are	the normalized x, y, z- perturbation velocities.

Fig. 4.4 shows the panel geometry representing the wing. For the upper surface, the perturbations on each panel of the aircraft can be expressed as:

$u_{top} = u_{thick} + u_{lift} + u_{vort} = U' + u_{vort}$,

$v_{top} = v_{thick} + v_{lift} - (dt/dx)/2 \sin\Theta - u_{vort} R_1 = V' - u_{vort} R_1$, and

$w_{top} = w_{thick} + w_{lift} + (dt/dx)/2 \cos\Theta - u_{vort} R_2 = W' - u_{vort} R_2$.

For the lower surface they can be expressed as:

$u_{bot} = u_{thick} + u_{lift} - u_{vort} = U' - u_{vort}$,
$v_{bot} = v_{thick} + v_{lift} + (dt/dx)/2 \sin\Theta + u_{vort} R_1 = V' + u_{vort} R_1$, and
$w_{bot} = w_{thick} + w_{lift} - (dt/dx)/2 \cos\Theta + u_{vort} R_2 = W' + u_{vort} R_2$.

In these expressions the subscripts $_{thick}$ and $_{lift}$ refer to the perturbations due to thickness and lift on the panels due to the other panels. R_1 and R_2 are the tangents of the vorticity in the YZ and the XY plane respectively:

$$R_1 = \frac{(Y2-Y1)\,(X3-X1-X4+X2+X2-X1)}{((Y2-Y1)^2+(Z2-Z1)^2)} \qquad R_2 = \frac{(Z2-Z1)\,(X3-X1-X4+X2+X2-X1)}{((Y2-Y1)^2+(Z2-Z1)^2)}.$$

For a planar wing these expressions are simplified: $w_{thick}=u_{lift}=v_{lift}=0$. We can now write the equation for $u_{vort,3D}$ based on local normal Mach number:

$$M_{2D} = M_{l,n,3D}$$
$$M_{2D}\, a_{3D} - U_{n,3D} = 0$$
$$M_{2D}^2 \left[1/M^2 + {}^1/_2(\gamma-1)\,(1-(1+u)^2-v^2-w^2)\right] - \left[\{(1+u)\cos\Lambda + v\sin\Lambda\}^2 + w^2\right] = 0$$
$$a\, u_{vort}^2 + b\, u_{vort} + c = 0$$

where:

$$a = -Q - Q R_1^2 - Q R_2^2 - C^2 - R_1^2 S^2 + 2 R_1 S C - R_2^2$$
$$b = -2Q + 2 V' R_1 Q + 2 W' R_2 Q - 2 C^2 + 2 V' R_1 S^2 + 2 R_1 S C + 2 U' R_1 SC + 2 W' R_2$$
$$c = M_{2D}^2/M^2 - 2 Q U' - Q U'^2 - Q V'^2 - Q W'^2 - C^2 - 2 U' C^2 - U'^2 C^2 - V'^2 S^2 - 2 V' S C - 2 U' V' SC - W'^2$$
$$Q = {}^1/_2(\gamma-1)\, M_{top}^2, \quad C = \cos\Lambda, \quad S = \sin\Lambda.$$

The solution is:
$$u_{vort,1,2} = \frac{-b \pm \sqrt{[b^2-4ac]}}{2a}.$$

The largest u root violates the small perturbation assumption, so we select the one with the smallest absolute value. Problems may occur when the actual normal Mach number of the panel is far from its design normal Mach number.

Fig. 4.4: Oblique wing sign conventions

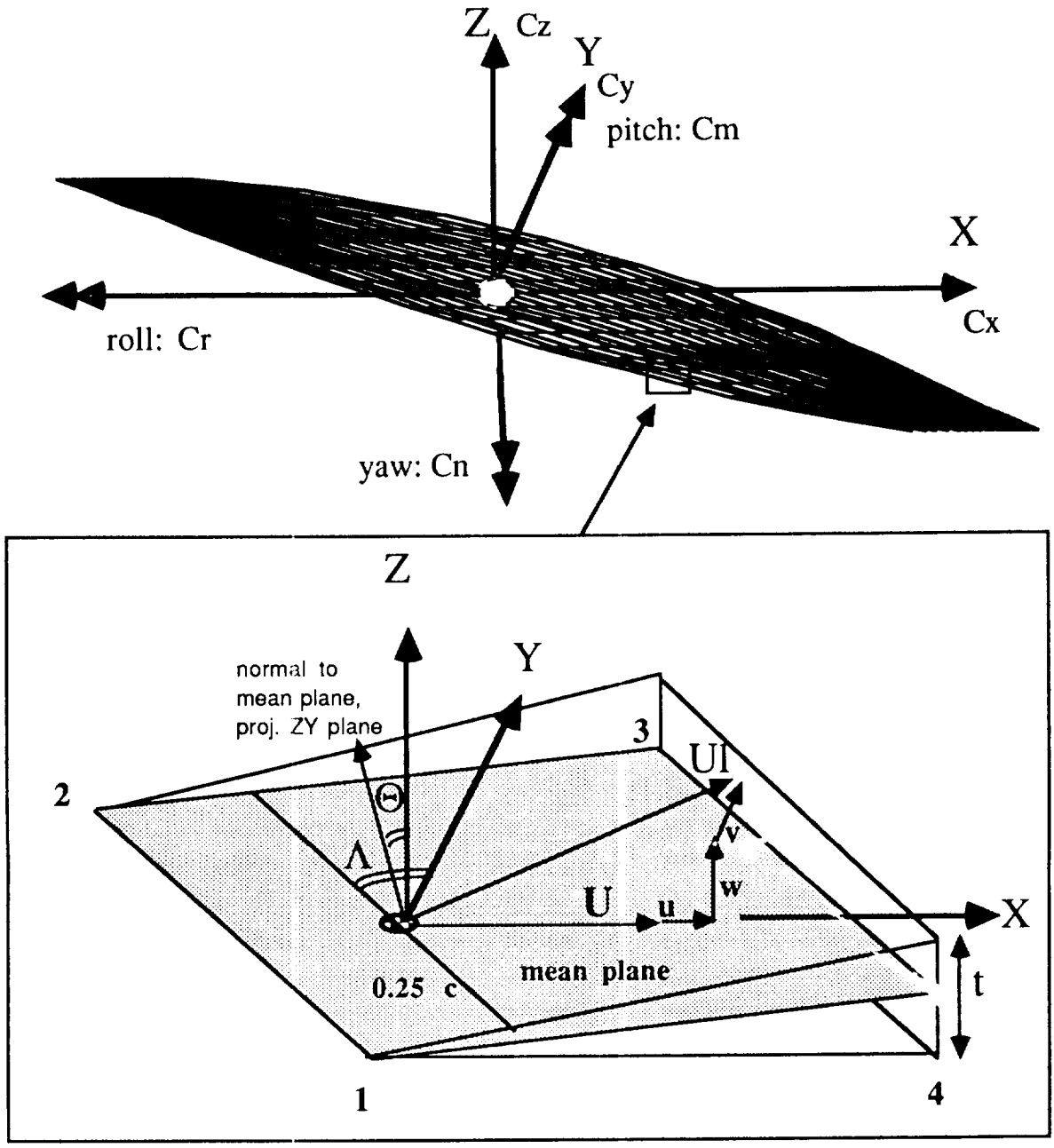

Panel with positive perturbations that satisfy the boundary conditions.

For example; when the normal component of the freestream Mach number on a panel exceeds 1.0 and a subsonic normal Mach number is prescribed on the top and the bottom of the panel, we are unable to resolve the discrepancy by changing the vorticity. Such problems can be solved by increasing the panel sweep.

We can now compute the target pressure distribution over the wing, using a first or a second order approximation:

First order: $C_p = -2u$

Second order: $C_p = M^2u^2+(1-U_l^2) = M^2u^2+1-[(1+u)^2+w^2+u^2]$.

The final perturbation U_l can be corrected with Riegel's correction [37] to improve the pressure coefficients estimates near the leading edge:

$U^2_{l,top,Riegels} = U_l^2/(1+((dt/dx)/2 + dz/dx)^2)$

$U^2_{l,bot,Riegels} = U_l^2/(1+((dt/dx)/2 - dz/dx)^2)$.

Which expression is superior depends on the code that is used to calculate the wing camber. If the code uses only the first order relation to determine the panel mean line slopes than we should use ΔC_p $(=4u_{vort})$ as input. The final result will still be second order accurate if the final perturbations are combined to a second order accurate pressure distribution. If the panel slopes are determined by higher order relations, the second order expression for ΔC_p should be used. The inverse code will return the required induced velocities and incidence (dz/dx) for each panel. These values are used for the next iteration. The perturbations to start the iteration can be obtained from an analysis of the wing with the original airfoil camber.

The panel code used in this paper was written by Ralph Carmichael and later modified by the authors for oblique wing research. The modifications include the method described in this paper and an improved drag calculation. The original code WING3D is based on work by Woodward [39] and Carmichael. WING3D solves the Prandtl-Glauert equation in subsonic and supersonic flow:

$$(1-M^2)\phi_{xx}+\phi_{yy}+\phi_{zz}=0.$$

The perturbations are defined as: $u=\delta\phi/\delta x$, $v=\delta\phi/\delta y$, $w=\delta\phi/\delta z$.

Sources, sinks and vortices that are distributed continuously over each panel are solutions

to the Prandtl Glauert equations. Since we know their induced velocity distribution in space, we can use them to construct the flow field around the wing. For this purpose an aerodynamic influence matrix [AI] containing the induced u-perturbations for each singularity is set up, inverted and multiplied through by a column vector representing the wing mean surface boundary conditions. In this way we obtain the u-perturbations at each panel:

$[4\, u_{vort}] = [\Delta CP] = [AI]^{-1} [dz/dx - \alpha]$.

It is also possible to solve for the wing camber if the u-perturbations are known:
$[dz/dx - \alpha] = [AI]\, [4\, u_{vort}]$.

Application of the Method

First we investigate the pressure distribution over a 16% thick airfoil with ARC2D, a Navier-Stokes code and WING3D, a potential flow code. Fig. 4.5a shows the pressure distribution at $\alpha = 3.3^{o}$ and Mach 0.6 calculated with ARC2D. We used a coarse 193 x 40 grid. There is a weak shock just aft of the leading edge. The center of pressure of this section is at 32% of the chord. Fig. 4.5b shows the pressure distributions calculated using WING3D with and without Riegel's correction. The distributions look similar to the one generated by ARC2D, though the pressures are a bit too high on the first part of the upper surface, resulting in an underprediction of the lift coefficient by about 7%, and the center of pressure is at 36% of the chord. In this case, probably due to the coarse panelling, Riegel's correction does not increase the accuracy. We will use the vorticity and the local normal Mach number distribution of the sections analyzed with the potential flow code for the inverse design. The reason the potential flow solution is preferred over the ARC2D solution can be easily understood in the two-dimensional case. If the pressure distribution from 4.5b were used to inversely design the camber distribution, we would get back the same airfoil. This airfoil would give the non-linear pressure distribution of Fig. 4.5a if it were analyzed with the ARC2D. To first order, this is also true for wings.

Next, we apply the method to the 72^{o} swept oblique flying wing SST. Fig. 4.6a shows an artist's impression of this transport. Because the normal component of the freestream Mach number changes as much as 0.4 from the leading to the trailing edge, the effective local sweep and taper must be included in the transformation. In addition, the low aspect ratio may induce significant three dimensional lateral velocities that change the local normal component of the flow.

One inverse design of the oblique flying wing was based on the method presented in the previous section and another used the simple sweep method. Both designs had a straight 32% chord line. Because the reference sweeps on the forward and aft wing are different, Boppe's method resulted in a wing with unequal lifts on the wing halfs. Forcing the normal Mach number to be the same everywhere on the wing, as Lock proposed, would be very difficult because of the large variation of the freestream normal Mach number component. For an elliptically loaded wing this would result in intolerable changes in the thickness distribution as well as large wave drag. We limited the number of panels with thickness representing the design to 400 to improve the condition number of the aerodynamic matrix and to reduce the computation time (20 panels of the same width in spanwise direction and 20 panels of the same fractional width in chordwise direction).

Fig. 4.6b shows the cruise pressure distribution. The suction peak on the upper surface decreases from the forward tip to the aft tip. This is because the sweep angle of the panel increases in this direction, and more suction is required to produce the same transonic normal Mach numbers. In Fig. 4.6d we see that the normal Mach numbers on the leading edge of the present method design are the same as for the airfoil, while the simple sweep design overshoots this target by as much as 0.1. The simple sweep design also has a weak shock near the 60% chord location of the aft tip. Fig. 4.6c shows that the control of the normal Mach number by the present method is achieved by varying the load distribution from tip to tip with respect to the simple sweep load distribution. The loading is decreased significantly on the leading edge of the forward tip and the 60% chord location of the aft tip. Because the center of the wing is untapered and the lateral induced velocities are small, its load distributions are very close to the distributions according to simple sweep theory.

In Fig. 4.6f the effective angle of attack of the mean surface is shown. The camber distribution resembles the linear antisymmetric distribution suggested by previous oblique wing research [20,29]. The forward-facing wing tip is substantially more cambered than the rearward-facing tip. Using the scaling factor, λ, we were able to produce a nearly elliptic load for a planar wing as shown in Fig. 4.6e.

4.4 The Calculation of Drag with Coarse Paneling

We designed the wing for target pressure distributions, but after this is done we still have to analyze the wings off design characteristics. If we use pressure integration to calculate the drag of wing, very dense paneling is required with any panel code. More than ten panels on the first 1% of the chord are needed to get the leading edge suction right, and

Fig. 4.5: The Pressure distribution of the OFWA 16

a. Analyzed with ARC2D. (193x40) grid
CL=0.81 Cm=-0.05 /alpha=3.3 deg., Mach=0.6

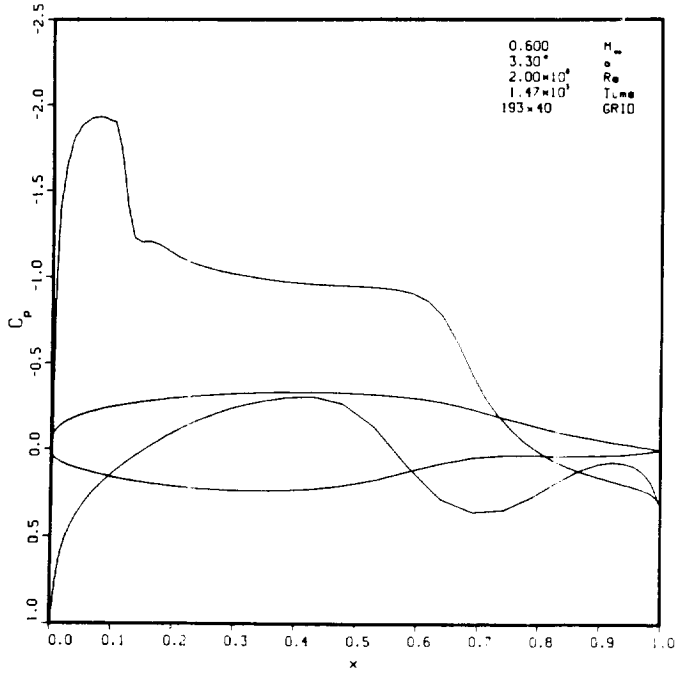

b. Analyzed with Wingbody. (20 panels + thickness)
CL=0.76 Cm=-0.08 /alpha=3.3 deg., Mach=0.6

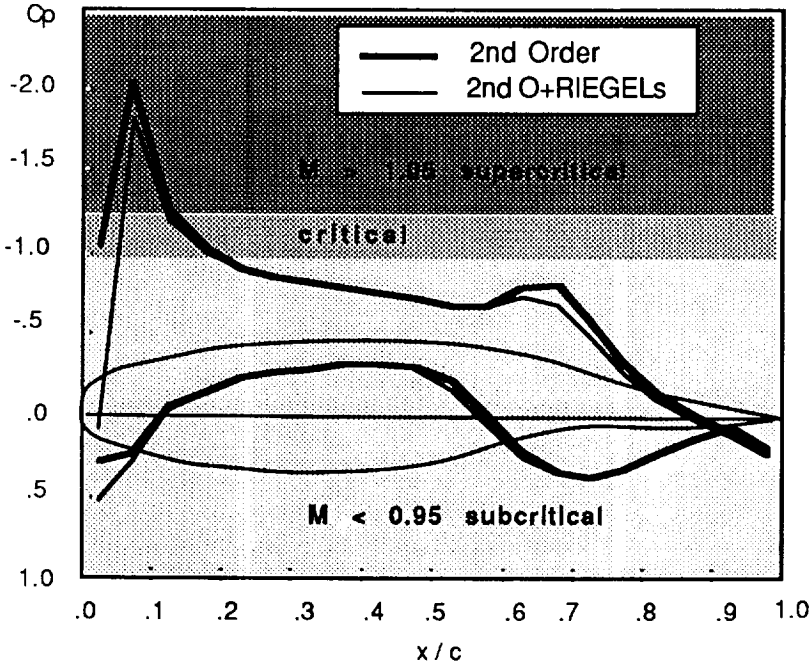

Fig. 4.6a: The oblique flying wing

b: Upper surface pressure distribution

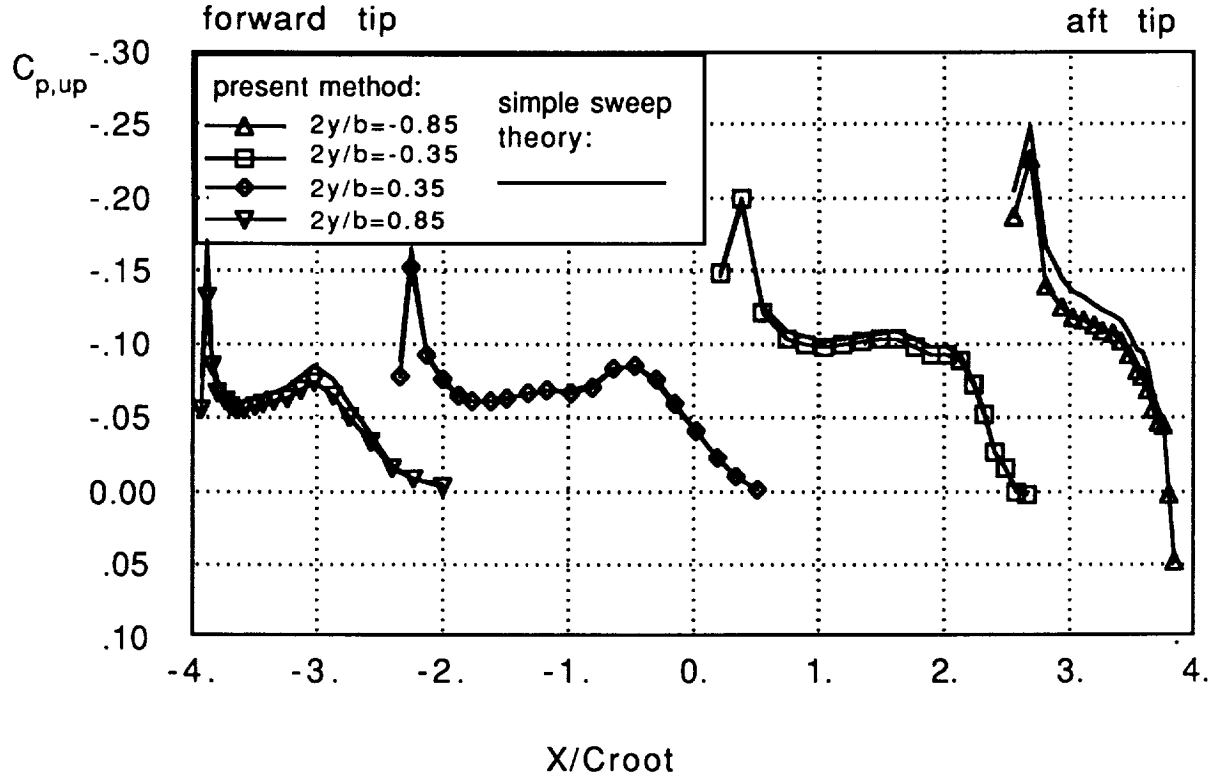

c: Chordwise load distribution

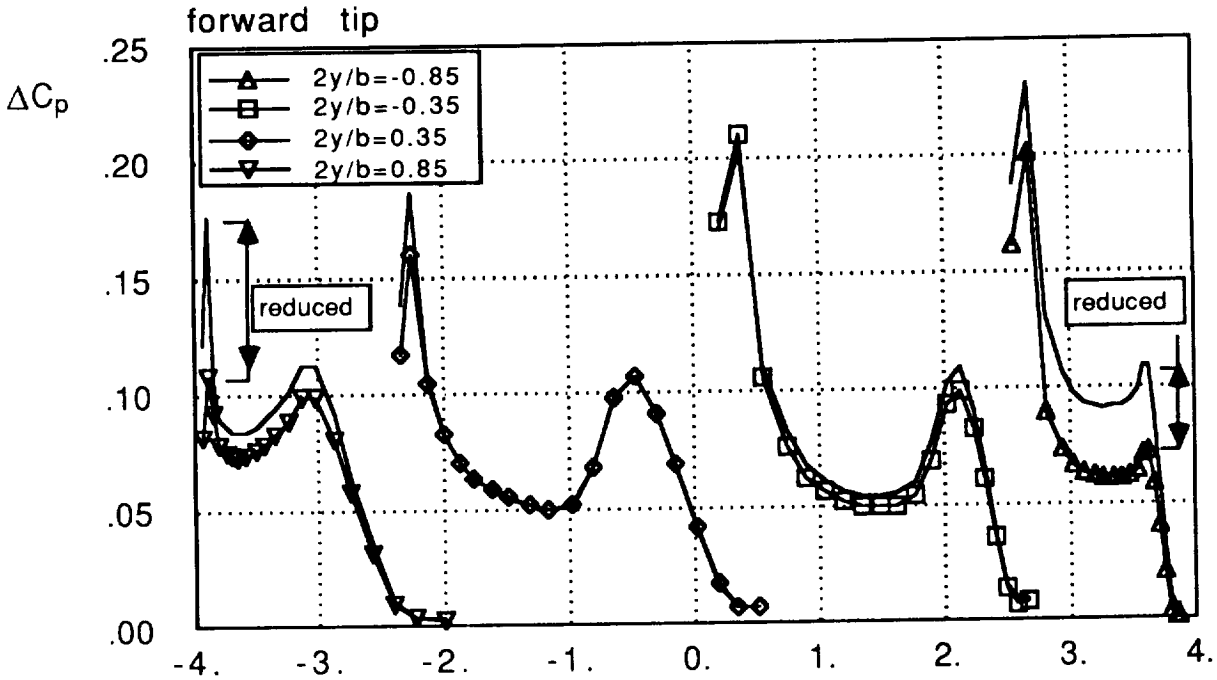

d: Upper surface normal Mach number distribution

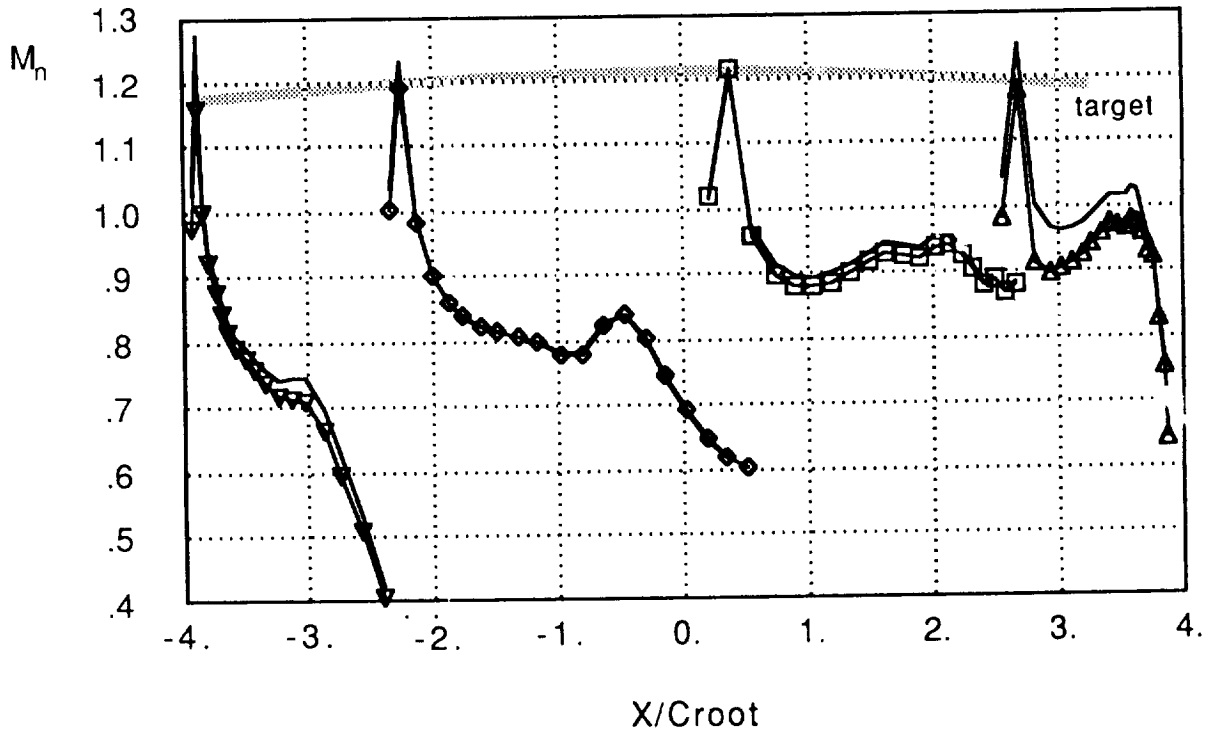

e: Spanwise load distribution

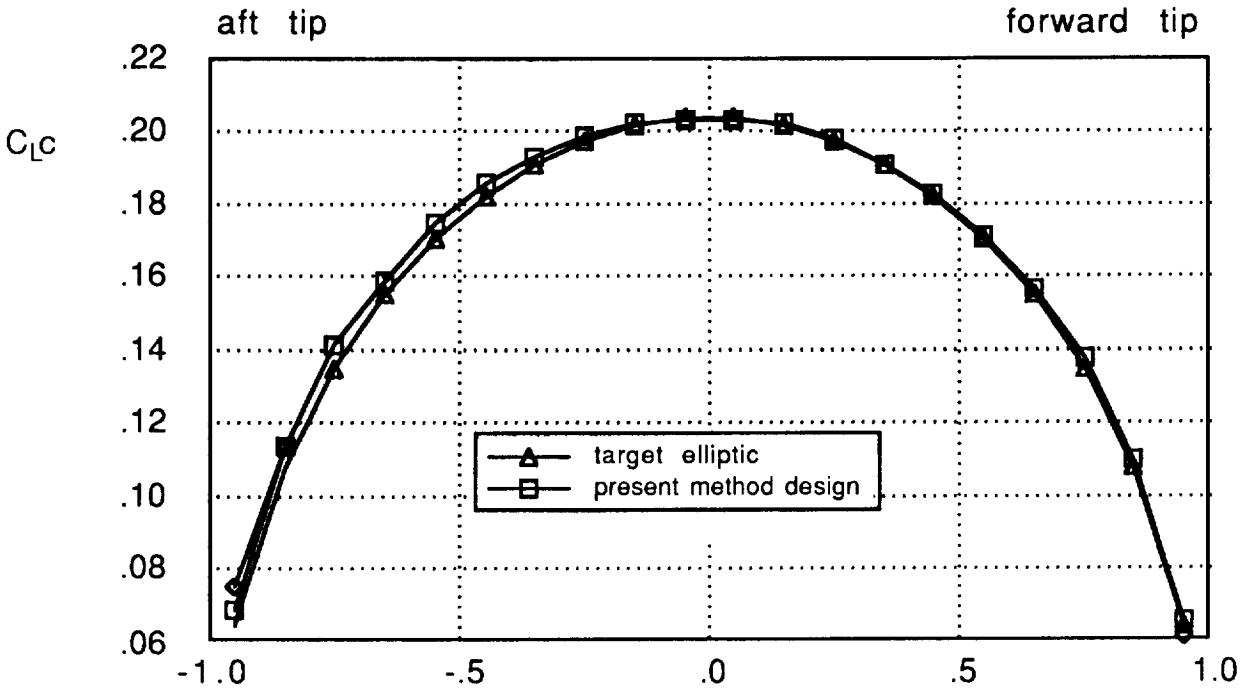

f: Camber distribution

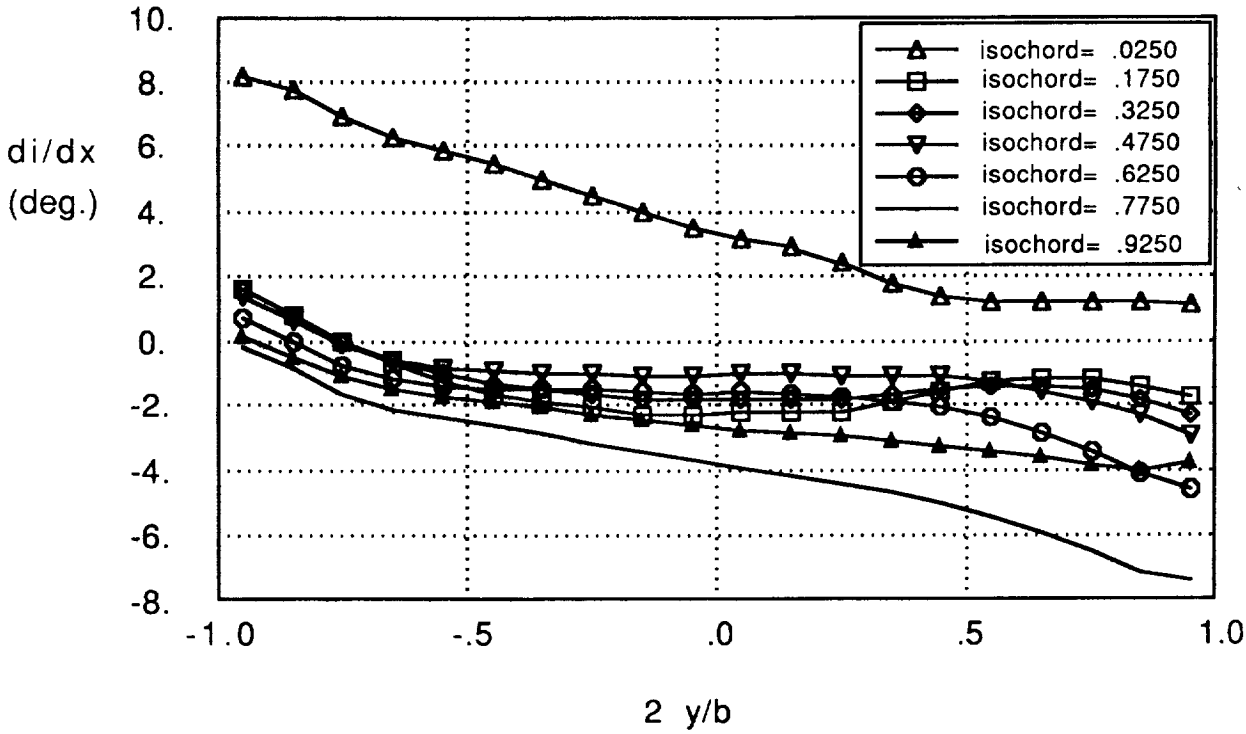

even with such fine paneling the induced drag cannot be predicted with an accuracy of more than about 10%. The Woodward code assumes that the wing is thin (i.e. dt/dx<1) and therefore additional errors would occur if we were to use fine paneling near a rounded nose. In this section we will investigate whether it is possible to get reasonably accurate results for the drag with coarse paneling.

Lift-dependent drag

The induced drag of each wing strip can be expressed as:

$$CDi/q=\sum_{i=1}^{n}(\Delta Cp_i \, dz/dx_i \, Area_i + \Delta T_{x,i_{le}}/q)$$

where: $Area_i$ is the projection of the panel area on the XYplane

$\Delta T_{x,i\ le}/q$ is the leading edge suction in X-direction

R.T. Jones [25] gives the following expression for the X and Y component of suction force on leading edge panels of wings with subsonic leading edges:

$$\Delta T_{x,i}/q= -2\pi\sqrt{(1-m^2)}\ \lim_{x\to xle} u^2(x-xle), \text{ and } \quad \Delta T_{y,i}/q=\Delta T_{x,i}/q \tan\Lambda$$

Multhopp [11] and Garner [9] evaluated this limit for incompressible flow assuming that u-perturbation on the chord is expressed in Fourier coefficients:

$$u=b/\pi c\,[\gamma\cot(\phi/2)+4\mu\{\cot(\phi/2)-2\sin\phi\}+\kappa\{\cot(\phi/2)-2\sin\phi-2\sin 2\phi\}..]$$

so; $$\lim_{x->xle} u^2(x-xle)=(b/\pi c)^2[\gamma+4\mu+\kappa.....]^2$$

The first two terms of this expansion can be related to the lift and pitching moment coefficients of a strip formed by the corner points of the panels over the length of the chord, as follows: $\gamma=CLc/2b$ and $\mu = CM_{1/4}c/2b$

In this expression the peturbations other than γ represent the u-distribution at the ideal angle of attack. Therefore, we could also write the limit as:

$$\lim_{x->xle} u^2(x-xle)=\frac{2c}{\pi}[C_L+\xi\, CM_{1/4}]^2 \qquad \xi=-[CL_i/CM_{1/4,ref}]$$

The variable ξ is the ratio of pitching moment to lift at the ideal angle of attack, e.g., the condition where u=0 on the leading edge. It should be evaluated with the same code and paneling as is used for the drag calculation. For a wing with a narrow chord it is reasonable to use the 2D value of ξ since there is not much induced camber. For wings with significant induced camber the value should be found by:

$$C_{L_i} = C_L \left[1 - \sqrt{1 + \frac{(CDi,ell - CDi,ref)}{CXsuc,ref}}\right]$$

The ref(erence) condition denotes the Mach number and angle of attack for which the wing loading is near elliptic, and full suction is assumed (ξ=0) Since this expression does not include wave drag due to volume, it can only be used for subsonic Mach numbers. Generally, a discontinuity in ξ is observed between subsonic and supersonic speeds. The supersonic value can be found by setting the induced drag equal on both sides of the speed of sound. The reference pitching moment is the weighted average pitching moment due to the u-perturbations around the quarter chord of the strips.

In Fig. 4.7a the lift-dependent drag for a flat straight wing, a flat delta wing and the OFW are compared with their theoretical values as presented in Ref. 14 and Ref. 2. The values predicted by the panel method correspond quite well up to Mach 3 .The induced drags of the OFW and the delta wing are about the same above Mach 2. If we unsweep the wing the induced drag can be significantly lower for speeds below Mach 2 (see also Fig. 2.5).

Volume-dependent drag

For thin wings the volume-dependent drag can be expressed as:

$$CDvol/q = \sum_{i=1}^{n} (Cp_t \, dt/dx_i \, Area_i) \qquad \text{and:} \quad Cp_t = -2\, u_{thick}$$

Fig. 4.7b gives the volume-dependent drag for a flat straight wing and a flat delta wing. The drag values are very close to those predicted by potential flow theory [14, 3]. For subsonic speeds the volume-dependent wave drag is correctly integrated to about zero. The oblique wing has a lower volume-dependent drag below Mach 2, but above this Mach number the drag rises sharply, while the volume-dependent drag of the delta wing keeps dropping. One could reduce the volume-dependent drag somewhat by sweeping the wing

further, but it would not be possible to keep the local normal Mach numbers transonic due to the effect of wing taper on the effective sweep of each panel.

4.5 Evaluation of the Forces and Moments

We can now analyze the OFW with the improved WING3D code. The sign convention is given in Fig. 4.4. All forces and moments were calculated on the basis of second-order pressure coefficients. The design condition for the wing analyzed with the linear potential flow code was C_L=0.07, $Cm_{0.32}$= -0.0035, and an elliptic lift distribution was required.

Fig. 4.8a shows that the lift increases linearly with angle of attack. The required cruise lift is achieved at the reference angle of attack (α=0). The potential drag (Fig. 4.8b) is within a few percent of the theoretical minimum given in Refs. 2 & 3. The wave drag due to volume 0.0013, and the lift-dependent drag value of 0.37 are very close to the values calculated earlier in the conceptual OFW study [41]. The side force (Fig. 4.18c) is the component in the Y-direction of the leading edge suction. It increases quadratically with the lift coefficient. The value of the sideforce is zero at cruise conditions, and is at most one percent of the value of the total lift at the off-design conditions.

At the cruise Mach number of 2, the pitching moment (Fig. 4.8d) is close to zero and the aircraft has a static margin of 0.13. At subsonic speeds, the static stability is almost neutral. The yawing moment (fig. 4.8e) reaches its minimum at the condition of elliptic loading. The yawing moment increases when the angle of attack is increased from the condition of elliptic loading. In this case, the increased upwash on the aft wing half tilts its lift-vector forward, which creates a positive yawing moment. The yawing moment also increases when the angle of attack is decreased from the condition of elliptic loading. When the angle of attack is decreased, the lift on the aft wing half is reduced much faster than the lift on the forward wing half. The resultant of the induced drag shifts in the positive Y-direction and creates a big positive yawing moment. The rolling moment (Fig. 4.8f) is almost zero at the required lift and increases with angle of attack because the rear wing loading increases due to the upwash from the forward wing half.

The lift-to-drag ratios presented in Fig 4.8g predict a maximum value around 11 for Mach 2.0, close to the values predicted by the method in Ref. 3 (point C in Fig. 2.2) for the same parasite drag.In Fig. 4.8h the relation between K and C_L is shown. At the design angle of attack, the lift distribution is more elliptical and the K factor approaches the theoretical minimum [2]. The force and moment curves are qualitatively similar to those published in Reference 6 of a highly swept oblique wing.

Fig. 4.7: Aerodynamic comparison for selected wings

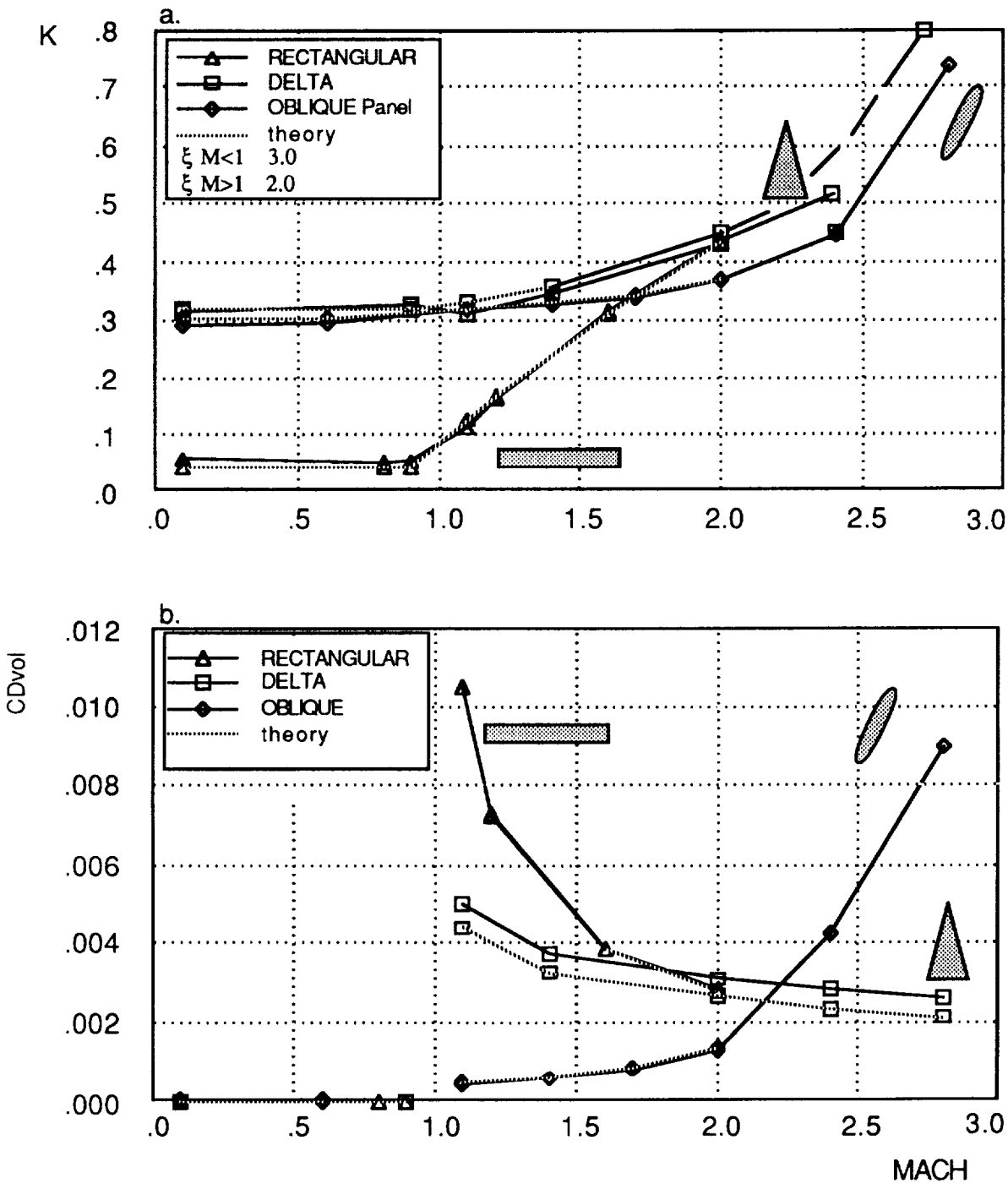

Fig. 4.8: Warped OFW in potential flow

Mach 2 AR=1.05 72.5 deg sweep
Cref= 2.4 Bref=2.5 Sref=6.1 / Xref=0.32c Yref=Center span

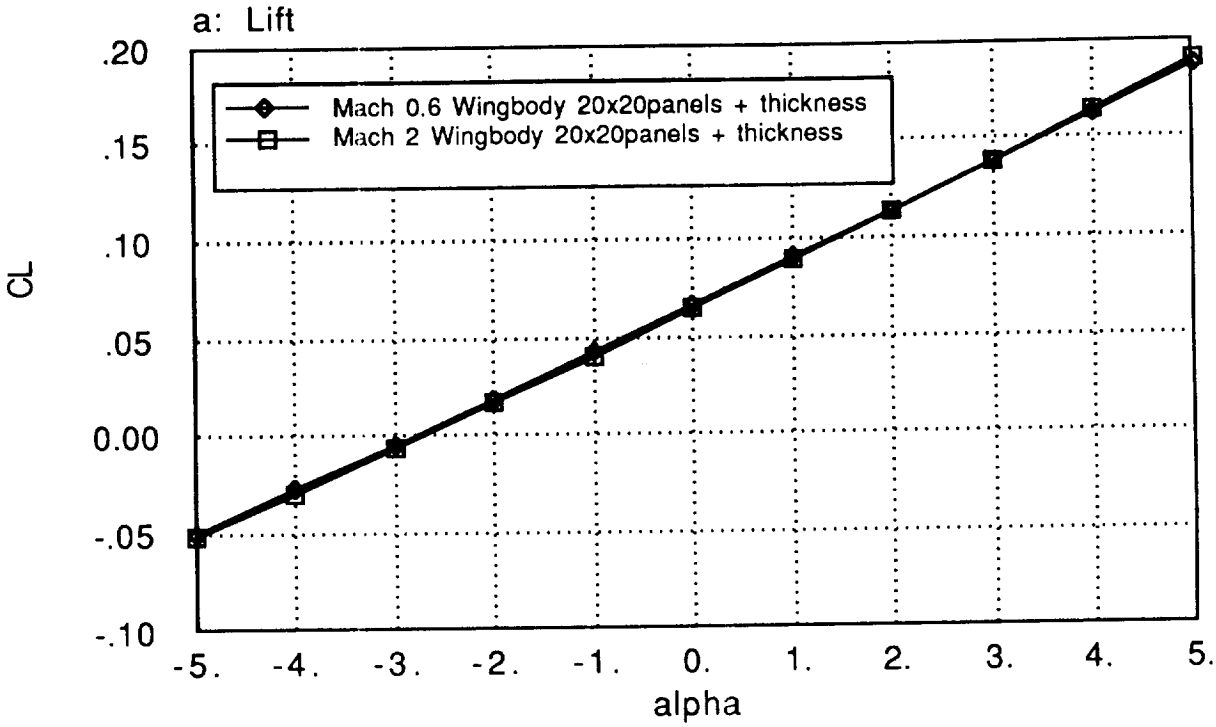

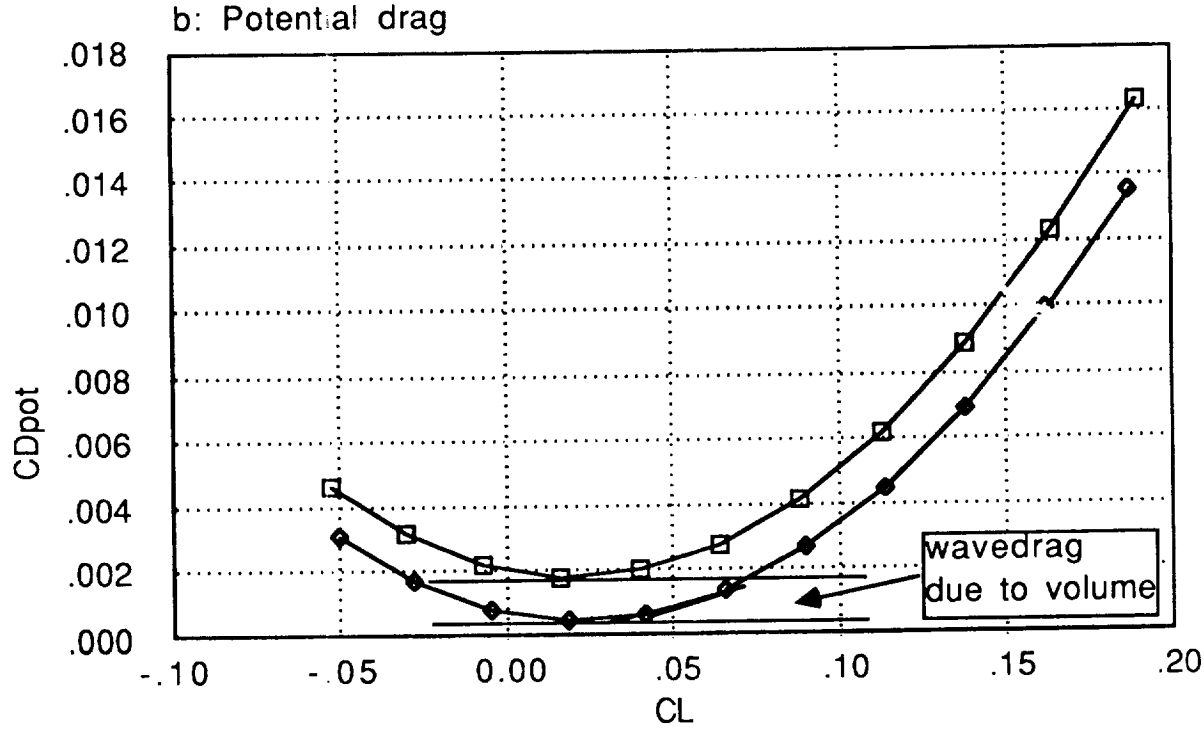

c: Side force

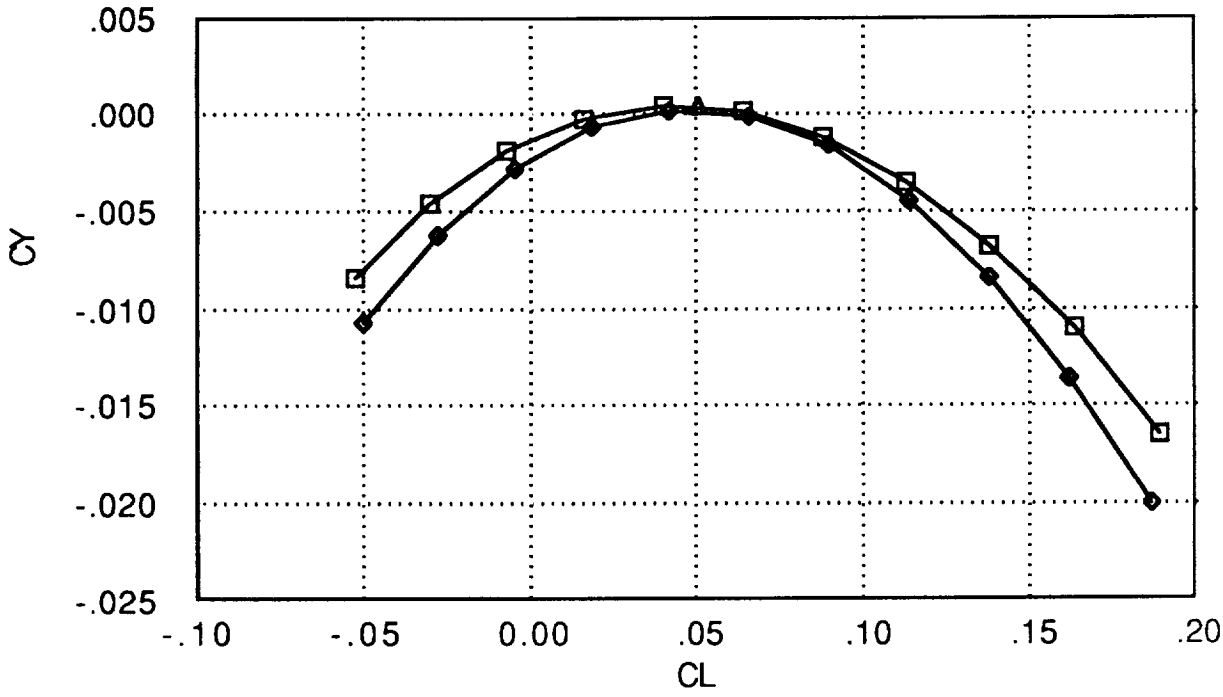

d: Pitching Moment

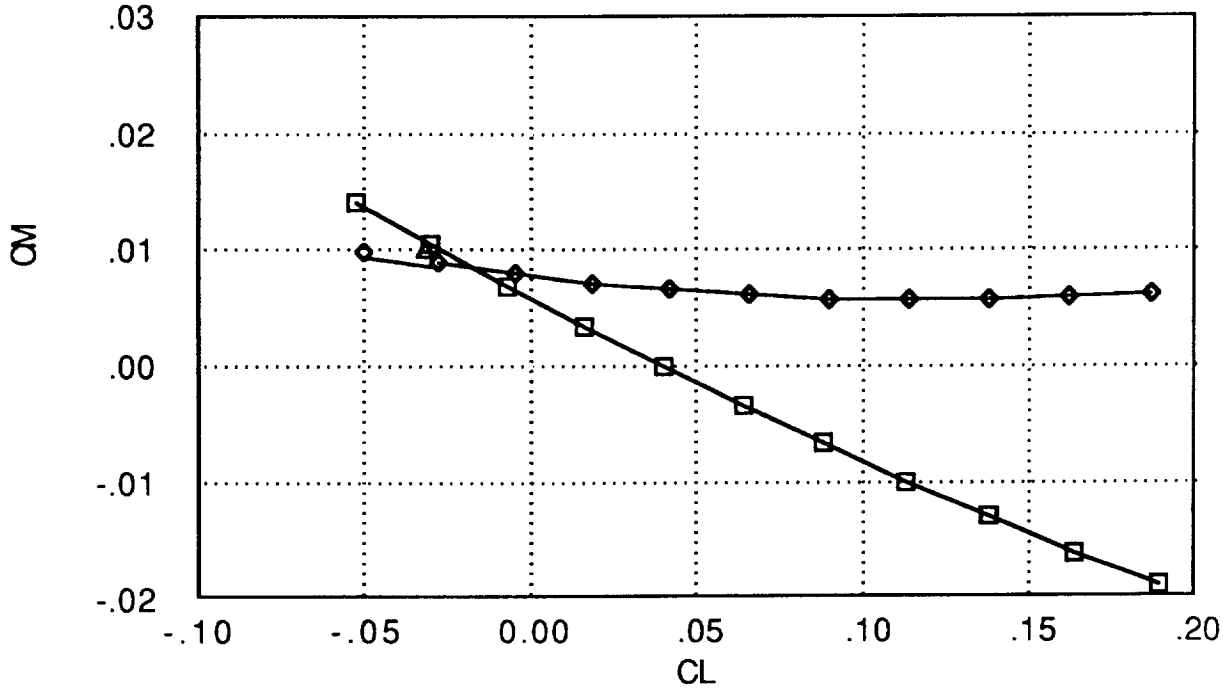

e: Yawing moment

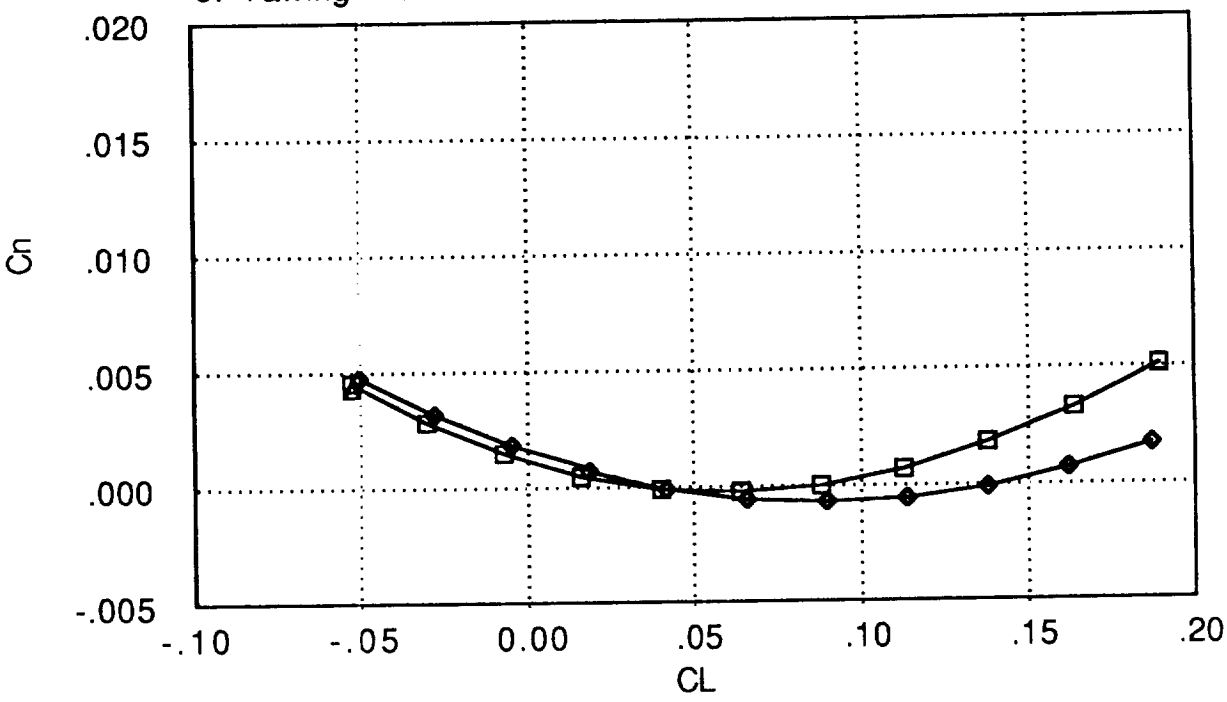

f: Rolling moment

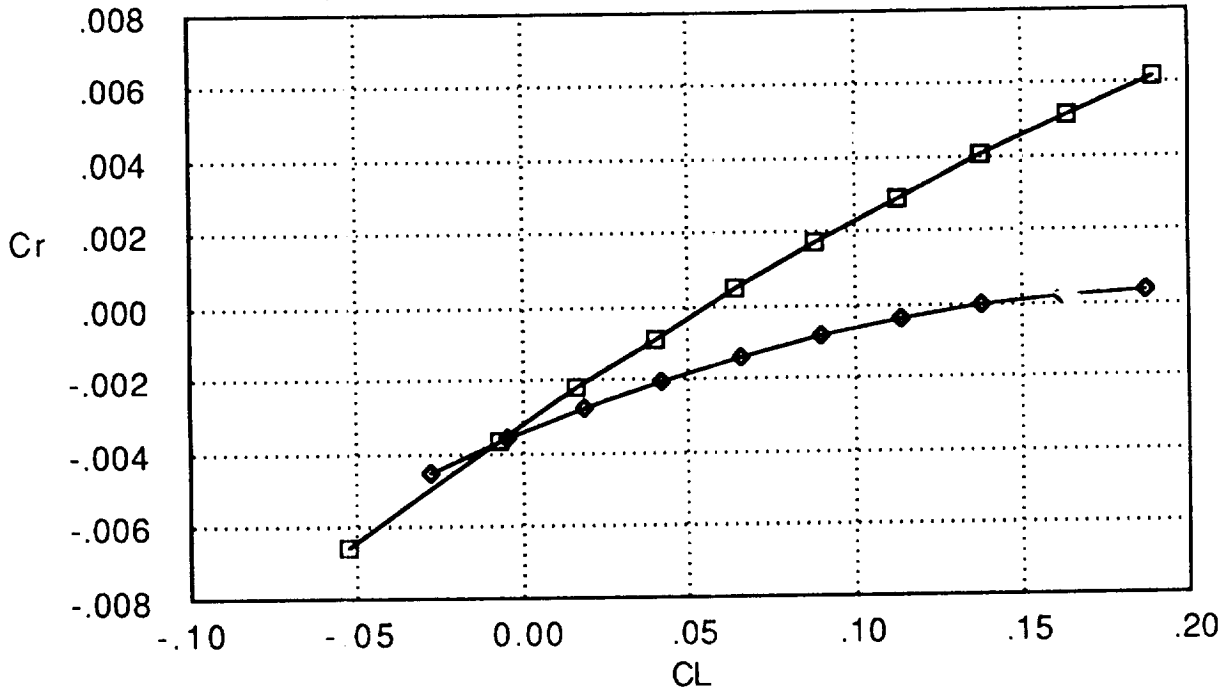

g: Lift-to-drag ratio with a parasite drag of 0.00413

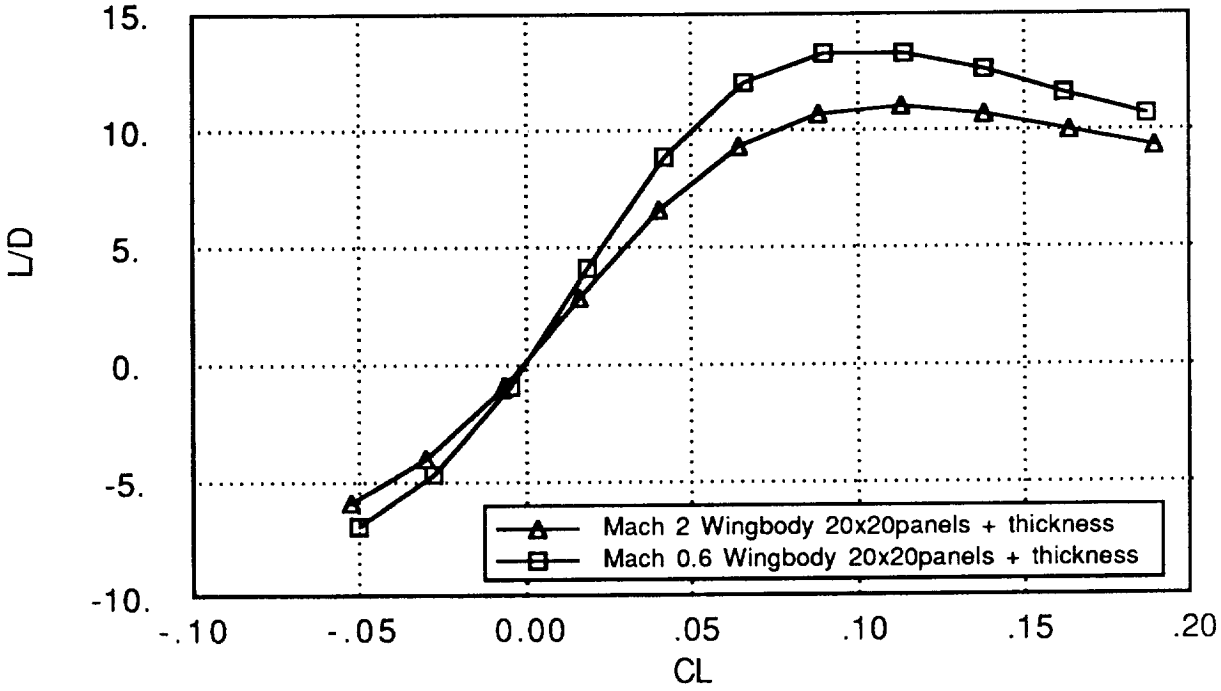

h: Lift dependent drag factor K

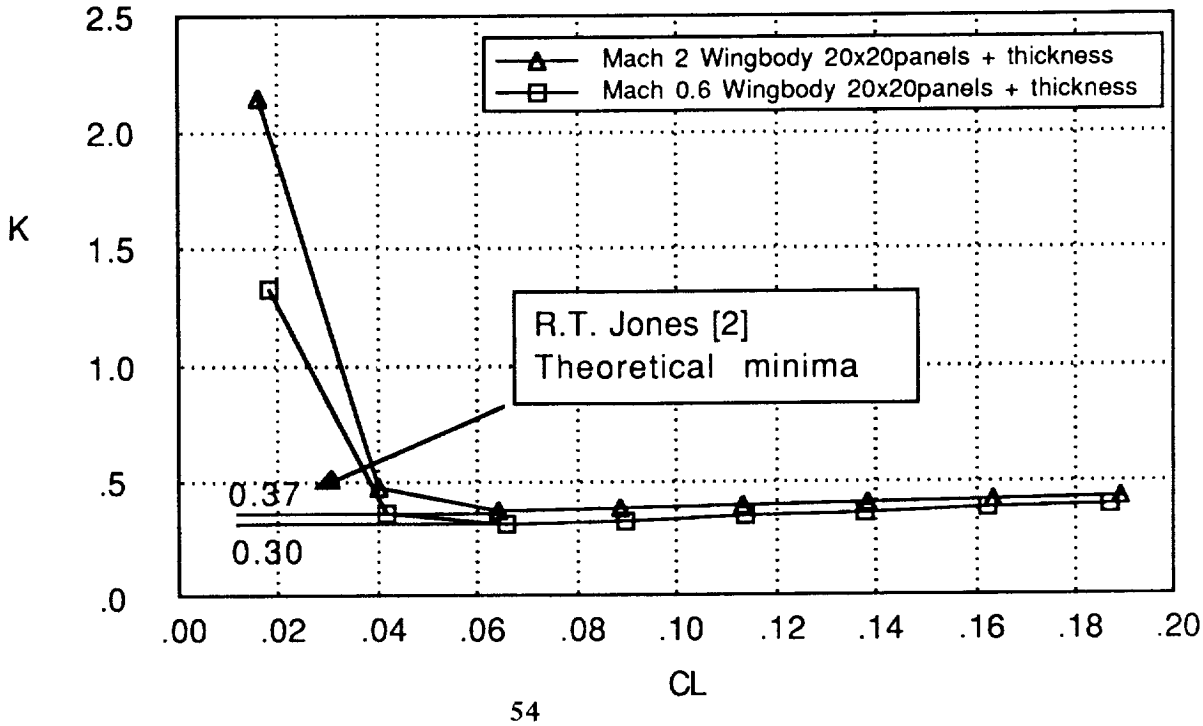

4.6 Control Authority

Control authority is the capacity to maneuver and trim the aircraft by generating moments and forces. One can obtain the desired pitching and rolling moments by deflecting the 10% trailing edge flap suitably along the span. In this way, the flap deflections can be directly used to control the aircraft by an artificial stability and control system. The required flap deflections are found by setting up a matrix with the partial derivatives of the rolling and pitching moments with respect to a suitable deflection along the span, inverting this matrix and then solving it for the required pitching and rolling moment. As an example we will calculate the symmetric deflection (s) and an asymmetric (negative on leading tip) deflection (a) required to balance the aircraft due to a 1 degree angle of attack change at CL=0.0065 and Mach 2:

$$\begin{bmatrix} s \\ a \end{bmatrix} = \begin{bmatrix} \delta Cm/\delta s & \delta Cm/\delta a \\ \delta Croll/\delta s & \delta Croll/\delta a \end{bmatrix}^{-1} \begin{bmatrix} CM\ required \\ Croll\ required \end{bmatrix} = \begin{bmatrix} -0.00435 & -0.00139 \\ 0.0053 & -0.0057 \end{bmatrix}^{-1} \begin{bmatrix} 0.00325 \\ -0.00100 \end{bmatrix} = \begin{bmatrix} 0.095 \\ -2.61 \end{bmatrix}$$

To trim the aircraft we need to deflect the flap at the leading tip 2.7° downward, and we need to deflect the flap at the trailing tip 2.5° upward. Between the trailing and leading tips the flap setting varies linearly. For a trimmed OFW, the lift gradient is 10% higher than for an untrimmed OFW and the induced drag remains approximately the same.

Recent research [27] has revealed that high side accelerations in pitch maneuvers are unacceptable to pilots. In the case of the OFW, for a 1.3 g pull-up maneuver at cruise a sidefore of 0.03g is created. This sideforce can be easily compensated by deflecting the two most inboard vertical tailplanes (shown in Fig. 1) in the same direction. Since each fin has an area of 1.7% of the wing planform and a lift gradient of 0.04 /°, we would only have to deflect them by 0.2°. However, higher side forces can be expected during subsonic maneuvering.

Yawing moments are generated by deflecting the fins on each wing half in opposite directions. The yawing moments due to changes in the angle of attack are of the same magnitude as the side force. But, the one engine out condition is the most important, and this condition dictated the size of the vertical fins as described in Ref. 41.The trailing fin gives the aircraft a directional stability of Cn_β=0.04/rad, slightly higher than the minimum value recommended in Ref.5.

Conclusions

An earlier study [41] suggested that the Oblique Flying Wing (OFW) would be economically attractive if it could achieve cruise lift-to-drag ratios that are comparable to those of other supersonic configurations. Because the OFW is able to adjust its sweep angle for each Mach number, it achieves a higher lift-to-drag ratio than any existing configuration up to Mach 2.0. Fig. 5.1 compares the lift-to-drag ratio of the OFW to that of the B747 and the Boeing High Speed Civil Transport [16].

The structural weight of the OFW will also be less than that of conventional configurations because the cabin is used as part of the wing. The wider span does not lead to a higher bending weight because the load is distributed over the span. (Fig 5.2).

Improvements in lift-to-drag ratios and empty weight will lead to better payload fractions. Since the payload fraction is directly related to Direct Operating Costs [15, 12] the improved payload fractions will result in lower DOC and therefore better economic performance. Fig. 5.3 compares the OFW and the 1989 HSCT designs on the basis of payload weight fractions. The OFW achieves payload fractions that are very close to that of the B747, while the HSCT configurations [34, 35] have significantly lower payload fractions.

Fig. 5.4 gives a general comparison between the Oblique Flying Wing, the current Boeing High Speed Civil Transport and the Boeing 747. We see that the OFW is lighter, carries the same payload and requires less runway than the B747, while being almost as fast as the HSCT.

Current and Future Work

Current research on the Oblique Flying Wing includes an environmental and an operational impact study. The research discussed for this paper and the current work was funded by NASA AMES.

Main Advantages of the Oblique Flying Wing

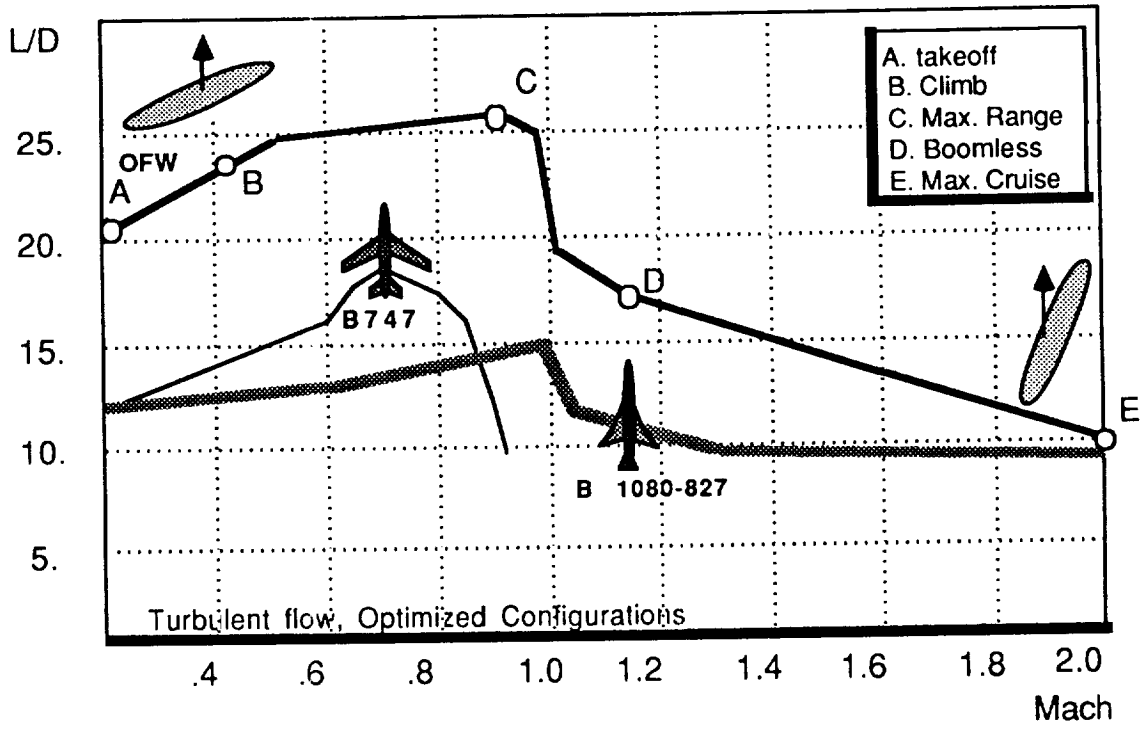

Fig. 5.1: The OFW has better performance and requires less fuel than other aircraft because it has higher lift-to-drag ratios.

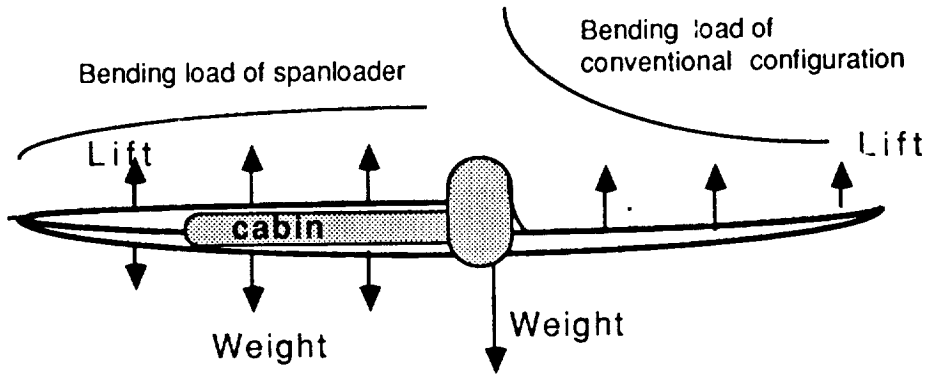

Fig. 5.2: The OFW has less structural weight than conventional configurations because the load is distributed over the span and the cabin is part of the wing.

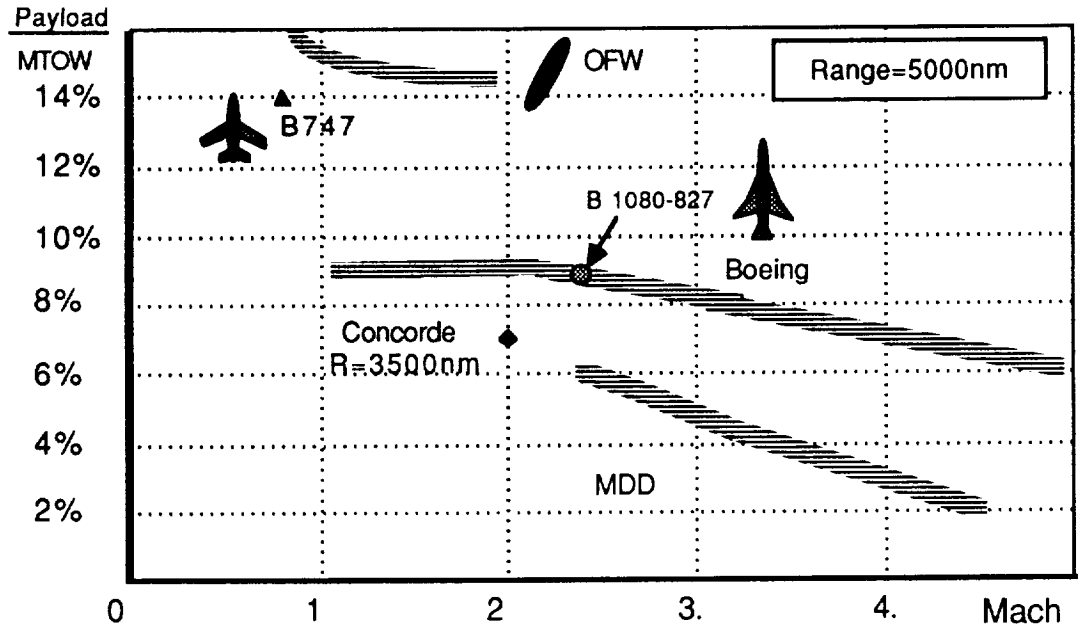

Fig. 5.3: The payload fraction of the OFW will be comparable to that of existing subsonic aircraft and 50% higher than that of the current High Speed Civil Transport designs.

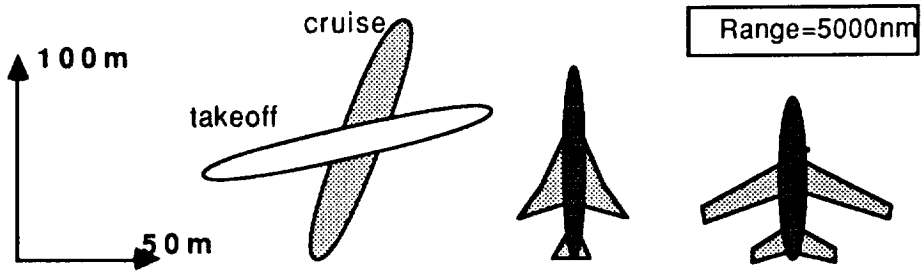

Type	OFW	B 1080-827	B747
Speed	Mach 2.0	Mach 2.4	Mach 0.85
Payload	462pax	247pax	452pax
Weight	300tons	340tons	360tons
Runway	2000m	3600m	3300m

Fig. 5.4: The OFW accommodates twice as many passengers, has less takeoff weight and requires only half the runway length of the current HSCT Boeing design.

References

1 **Jones, R.T.** 'The supersonic flying wing', Aerospace America, october 1987

2 **Jones, R.T.** 'High Speed Wing Theory' Princeton Aeronautical Paperbacks 1960

3 **Smith, J.H.B.** 'Lift/drag ratios of optimized slewed elliptic wings at supersonic speeds' The Aeronautical Quarterly. Vol. 12 pp. 201-218 August 1961

4 **Van Der Velden, A.** 'Design of a Small Supersonic Oblique-Wing Transport Aircraft' Journal of Aircraft Vol 26,#3 March 1989 Also Engineer's thesis U. of Technology Delft, 1986, 318pp

5 **Torenbeek E.,** 'Synthesis of subsonic aircraft design', Student edition, Delft University of Technology/Martinus Nijhoff, 1982

6 **Jones, R.T et alli** 'An experimental investigation of three oblique wing and body combinations', NASA TM-X-62256, 1973

7 **Wittenberg H.** Notes:'Propulsion of Aircraft' University of Technology Delft. (In Dutch) Dictaat D-32A 1983

9 **Garner H.C.** 'Some remarks on vortex drag and its spanwise distribution in incompressible flow' JRAeS vol 72 pg624

10 **Kuchemann, D.,** 'Aerodynamic design of aircraft', Pergamon Press

11 **Multhopp H.** 'Methods for calculating the lift distribution of wings' R&M 2884 Jan 1950

12 **Van Der Velden, A.** 'An economic model to evaluate high-speed transport aircraft designs', NASA CR177530.

13 **Lee G.H.,** 'Slewed Wing Supersonics',The Aeroplane, March 1961.

14 **Schlichting/Truckenbrodt** 'Aerodynamik des Flugzeuges' zweiter band Springer Verlag Berlin 1969

15 **Torenbeek E.** 'Fundamentals of Conceptual design optimization of subsonic transport Aircraft', Delft University of Technology dept. of Aerospace Eng. 1980.

16 **Boeing C. A.** 'High-Speed Civil Transport Study'.NASA CR 4233, 9-'89

17 **Head M.R** 'Entrainment in Turbulent Boundary Layers', British Aeron. Research Committee, reports and memo 3152, 1960

18 Van der Velden,A. 'Design of Oblique, Swept and Delta Wing Supersonic Aicraft', Unpublished Delft University of Technology, 1985 parametric investigation including:'Boeing 1-2a, 3-2a, 5-3a, SXJET,Concorde,MDD AST,SCAT 15F'

19 Jones, R.T 'Theory of wing-body drag at supersonic speeds' NACA Report 1284

20 Kroo, I 'The Aerodynamic Design of Oblique Wing Aircraft' AIAA-86-2624 AIAA/AHS/ASEE Aircraft Systems Design and Technology Meeting October 20-22 1986 Dayton Ohio

21 Eminton, E 'On the numerical evaluation of the drag Integral' RAE RM 3341, 1961

22 Harvard, L. 'The wave drag of arbitrary configurations in linearized flow as determined by areas and forces in oblique planes. NACA RM A55A18 TIB 4620, March 1955

23 Lock, R.C 'An equivalence Law Relating Three- and Two Dimensional Pressure Distributions'. RAE Reports and Memoranda 3346 May 1962

24 Pulliam,T 'Efficient Solution Methods for the Navier-Stokes Equations'. Lecture notes for the Von Karman Institue for fluid dynamics lecture series: Brussels Jan 1986

25 Jones,R.T. 'Aerodynamic design for supersonic speed'. Advances in aeronautical sciences. vol 1. Pergamon Press 1959

26 Mehta, U. 'The computation of flow past an oblique wing using the thin-layer Navier-Stokes equations. Nasa TM 88317 1986

27 Kempel R., McNeill W., Gilyard G.B, Maine T.A
'A piloted Evaluation of an Oblique-Wing Research Aircraft Motion Simulation With Decoupling Control Laws'
NASA TP 2874 Nov. 1988

28 Ward. G.N. 'Linearized theory of steady high-speed flow.'Cambridge University press 1948

29 Rockwell 'Oblique Wing Research Aircraft Phase B Preliminary Design'. Rockwell Intl. 15 April 1987

30 Liepmann, H.W, Roshko, A.
'Elements of Gasdynamics', Galcit aeronautical series, 1957

34 Graf, D.A.,Stroup, J.W.
'Economic feasibility of high-speed civil transports:,AIAA Aircraft design and operations meeting, Atlanta Georgia. Sept 7-9. 1988

35 Morris, C., Winston, M., Morris, S.
'Some key considerations for high-speed civil transports'. AIAA-88-4466

36 Boppe, C.W 'X-29 Aerodynamic Design and Performance' AIAA Professional Study Series - Aerodynamic Analysis and Design 6,7 October 1988 Palo Alto

37 Riegels,F.W. 'Airfoil sections'London, Butterworths 1961

38 Tinoco, E.N 'Recent applications of CFD at Boeing' Professional Study Series - Aerodynamic Analyis and Design 6,7 October 1988 Palo Alto California

39 Woodward, F.A. 'Analysis and Design of Wing-Body Combinations at Subsonic and Supersonic Speeds'. Journal of Aircraft vol 5. no 6 1968

41 Van der Velden, A. 'The Conceptual Design of a Mach 2 Oblique Flying Wing Supersonic Transport', NASA CR177529 May 1989

42 Swan, W.C 'A discussion of selected aerodynamic problems on integration of systems with airframe on transport aircraft' Boeing Co

43 Czarnecki,K.R, Sevier,J.R.
'Investigation of effects of distributed surface roughness on a turbulent boundary layer over a body of revolution at a Mach number of 2.01' NACA 4183, 1958

44 Fiecke, D. 'Die Bestimmung der flugzeugpolaren fuer entwurfszweke' DVL 1956

45 Butler,S.F. 'Aircraft drag prediction for project appraisal and performance estimation' AGARD CP124 1973

46 Czarnecki,K.R. , Sevier,J.R. , Carmel,M.M.
'Effects of fabrication type roughess on turbulent skin friction at suprsonic speeds' NACA TN 4299

48 Lock,R.C. 'The aerodynamic design of winged aircraft at transsonic and supersonic speeds'. Journal of the Royal Aeronautical society June 1963

Software References

The following software tools were used for the parametric studies:

AVSAD (by A.J.M. Van der Velden, TUDelft/UC Berkeley/Stanford U Pascal, IBM XT) General parametric configuration design program Detailled description in Chapter 2 -*code made available upon request*

The airfoil was designed with the following software:

PANDA (by. I.Kroo, Stanford AA, Fortran, MacII):
Interactive inviscid analysis of a 2D airfoil by Riegels Method. Weber R&M 3026, a modification for thin airfoil theory. 180 points to define the airfoil. -*code available from author*

ARC2D (by T.Pulliam, NASAS AMES, Fortran, CRAY XMP)
Solution of the Euler and thin layer Navier Stokes equation. The airfoil was defined with a 193x40 C-grid generated by HYGRID and later with a 500x100 C-grid , first mesh point 5e-7c from the wall for the NS solution.

LBAUER (by L.Bauer, Fortran, VAX)
Solves the 2D linear potential equation for transsonic flow over the airfoil geometry + boundary layer. We used an 160x80 O-grid.

To design and analyse the 3D Oblique Flying Wing the following software tools were developed:

WAVE (by A.J.M. Van der Velden, Stanford AA, Fortran, MacII)
Eminton Lord code voor volume-dependent wave drag
-*code made available upon request*

PANEL (by A.J.M. Van der Velden, Stanford AA, Fortran MacII)
Panneling of configurations based on arbitrary input corner points and defined transformation and transformation of 2D-->3D pressure distributions with second order CP's. Output for Wing3D, SHADE and QUICKPLOT-*code made available upon request*

WING3D (by R. Carmichael, modified by Van der Velden, Fortran, MacII VAX)
Woodward linear potential flow code for subsonic and supersonic flow, with second order pressure distributions and leading edge suction correction. -*code made available upon request*

Aknowledgements

The authors wish to thank prof. Dr. Harvard Lomax and Dr. Unmeel Metha of the Fluid Dynamics Division of NASA AMES, Ralph Carmichael of the Aerodynamics Division of NASA AMES and prof. Dr. Robert T. Jones of Los Altos for their assistance in the completion of this work. Special thanks to Dr Evelin Sullivan for improving this paper.

NASA
National Aeronautics and Space Administration

Report Documentation Page

1. Report No.	2. Government Accession No.	3. Recipient's Catalog No.
NASA CR-177552		

4. Title and Subtitle	5. Report Date
The Aerodynamic Design of the Oblique Flying Wing Supersonic Transport	June 1990
	6. Performing Organization Code

7. Author(s)	8. Performing Organization Report No.
Alexander J. M. Van Der Velden and Ilan Kroo	A-90168
	10. Work Unit No. 505-60

9. Performing Organization Name and Address	11. Contract or Grant No.
Stanford University Palo Alto, California 94053	NCA2-343
	13. Type of Report and Period Covered Contractor Report

12. Sponsoring Agency Name and Address	14. Sponsoring Agency Code
National Aeronautics and Space Administration Washington, DC 20546-0001	

15. Supplementary Notes

Point of Contact: Unmeel Mehta, Ames Research Center, MS 202A-1, Moffett Field, CA 94035-1000
(415)604-5548 or FTS 464-5548

16. Abstract

The aerodynamic design of a supersonic oblique flying wing is strongly influenced by the requirement that passengers must be accommodated inside the wing. Recent research has revealed that thick oblique wings of very high sweep angle can be efficient at supersonic speeds when transonic normal Mach numbers are allowed on the upper surface of the wing. The present work was motivated by the ability to design a maximum thickness, minimum size oblique flying wing.

To achieve these goals, we used a 2D Navier-Stokes solver to design airfoils up to 16% thickness with specified lift, drag and pitching moment. A new method was developed to calculate the required pressure distribution on the wing based on the airfoil loading, normal Mach number distribution and theoretical knowledge of the minimum drag of oblique configurations at supersonic speeds. Using an inverse potential flow solver we calculated the wing mean surface for this pressure distribution.

The lift-to-drag ratio of this wing was significantly higher than that of a comparable delta wing for cruise speeds up to Mach 2.

17. Key Words (Suggested by Author(s))	18. Distribution Statement
Oblique, Flying wing, Supersonic transport aircraft, Computational fluid dynamics, Transonic airfoil design, Wing design	Unclassified—Unlimited Subject category—05

19. Security Classif. (of this report)	20. Security Classif. (of this page)	21. No. of Pages	22. Price
Unclassified	Unclassified	69	A04

For sale by the National Technical Information Service, Springfield, Virginia 22161